Contents

Chapter 1

Introduction

Problems of interface growth have received much attention recently [1–3]. Such are, for example, the duffusion limited aggregation (DLA) [4], random sequential adsorption (RSA) [5], Laplacian growth [6–8] or flame front propagation [9]. We will mainly pay attention in this Thesis to the numerical and analytical investigation of the last two problems. In addition to the fact that flame front propagation is an interesting physical problem we feel that we can also explain experimental results on the basis of theoretical investigations. There exists possibility to use methods found for the flame front propagation, in different fields where similar problems appear such as the important model of Laplacian growth .

The premixed flame - the self-sustaining wave of an exothermic chemical reaction - is one of the basic manifestations of gaseous combustion. It is well established, however, that the simplest imaginable flame configuration - unbounded planar flame freely propagating through initially motionless homogeneous combustible mixture - is intrinsically unstable and spontaneously assumes a characteristic two- or three-dimensional structure.

In the recent paper of Gostintsev, Istratov and Shulenin [10] an interesting survey of experimental studies on outward propagating spherical and cylindrical flames in the regime of well developed hydrodynamic (Darrieus-Landau) instability is presented. The available data clearly indicate that freely expanding wrinkled flames possess two intrinsic features:

1. Multi-quasi-cusps structure of the flame front. (The flame front consists of a large number of quasi-cusps, i.e., cusps with rounded tips.)

2. Noticeable acceleration of the flame front

Moreover, the temporal dependence of the flame radius is nearly identical for all premixtures discussed and correlates well with the simple relation:

$$R_0(t) = At^{3/2} + B \tag{1.1}$$

Here $R_0(t)$ is the effective (average) radius of the wrinkled flame and A, B are empirical constants.

In this Thesis we study the spatial and temporal behavior of a nonlinear continuum model (i.e., a model which possesses an infinite number of degrees of freedom) which embodies all the characteristics deemed essential to premixed flame systems; namely, dispersiveness, nonlinearity and linear instability. Sivashinsky, Filyand and Frankel [11] recently obtained

an equation, denoted by SFF in what follows, to describe how two-dimensional wrinkles of the cylindrical premixed flame grow as a consequence of the well-known Landau-Darrieus hydrodynamic instability. The SFF equation reads as follows:

$$\frac{\partial R}{\partial t} = \frac{U_b}{2{R_0}^2(t)} \left(\frac{\partial R}{\partial \theta} \right)^2 + \frac{D_M}{{R_0}^2(t)} \frac{\partial^2 R}{\partial \theta^2} + \frac{\gamma U_b}{2R_0(t)} I\{R\} + U_b \ . \tag{1.2}$$

where $0< \theta < 2\pi$ is an angle, R(θ,t) is the modulus of the radius-vector on the flame interface, U_b, D_M, γ are constants.

$$I(R) = \frac{1}{\pi} \sum_{n=1}^{\infty} n \int_0^{2\pi} cos[n(\theta - \theta^*)] R(\theta^*, t) d\theta^* =$$

$$= -\frac{1}{\pi} P \int_{-\infty}^{+\infty} \frac{\frac{\partial R(\theta^*,t)}{\partial \theta^*}}{\theta^* - \theta} d\theta^* \tag{1.3}$$

$$R_0(t) = \frac{1}{2\pi} \int_0^{2\pi} R(\theta, t) d\theta \ . \tag{1.4}$$

Sivashinsky, Filyand and Frankel [11] made a direct numerical simulation of this nonlinear evolution equation for the cylindrical flame interface dynamics. The result obtained shows that the two mentioned experimental effects take place. Moreover, the evaluated acceleration rate is not incompatible with the power law given by eq.(1.1). For comparison, numerical simulations of freely expanding diffusively unstable flames were presented as well. In this case no tendency towards acceleration has been observed.

In the absence of surface tension, whose effect is to stabilize the short-wavelength perturbations of the interface, the problem of 2D Laplacian growth is described as follows

$$(\partial_x^2 + \partial_y^2) u = 0 \ . \tag{1.5}$$

$$u \mid_{\Gamma(t)} = 0 \ , \partial_n u \mid_{\Sigma} = 1 \ . \tag{1.6}$$

$$v_n = \partial_n u \mid_{\Gamma(t)} \ . \tag{1.7}$$

Here $u(x, y; t)$ is the scalar field mentioned, $\Gamma(t)$ is the moving interface, Σ is a fixed external boundary, ∂_n is a component of the gradient normal to the boundary (i.e. the normal derivative), and v_n is a normal component of the velocity of the front.

To obtain results for radial flame growth it is necessary to investigate the channel case first. The channel version of equation for flame front propagation is the so-called Michelson-Sivashinsky equation [12, 13] and looks like

$$\frac{\partial H}{\partial t} = \frac{1}{2} \left(\frac{\partial H}{\partial x} \right)^2 + \nu \frac{\partial^2 H}{\partial x^2} + I\{H\} \ . \tag{1.8}$$

$$I(H) = -\frac{1}{\pi} P \int_{-\infty}^{+\infty} \frac{\frac{\partial H(x^*,t)}{\partial x^*}}{x^* - x} dx^* \ . \tag{1.9}$$

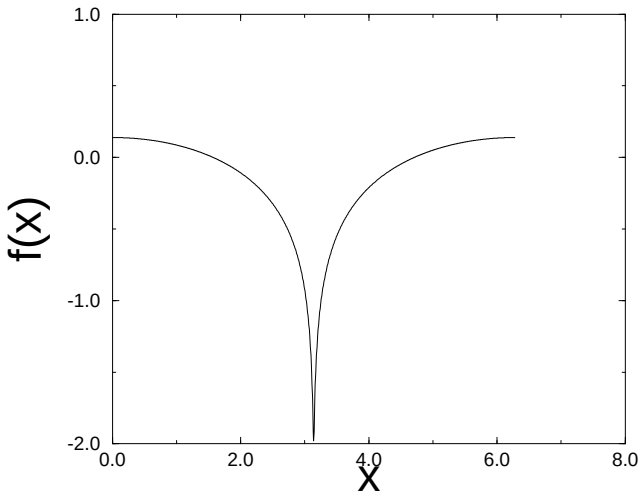

Figure 1.1: Giant cusp solution

with periodic boundary condition on the interval x [0,L], where L is size of the system. ν is constant, $\nu > 0$. H is the height of the flame front point, $P\int$ is the usual principal value integral.

Equations for flame front propagation and Laplacian growth with zero surface tension have remarkable property : these equations can be solved in terms of poles in the complex plane [6, 12, 14–16]. So we obtain a set of ordinary differential equations for the coordinates of these poles. The number of the poles is constant value in the system, but to explain such effect as growth of the velocity flame front we need to consider some noise that is a source of new poles. So we need to solve the problem of interaction of the random fluctuations and the pole motion.

The simplest case is the channel geometry. Main results for this case is existence of the giant cusp solution [12](Fig.1.1), which is represented in configuration space by poles which are organized on a line parallel to the imaginary axis. This pole solution is an attractor for pole dynamics.

A complete analysis of this steady-state solution was first presented in Ref. [12] and the main results are summarized as follows:

1. There is only one stable stationary solution which is geometrically represented by a giant cusp (or equivalently one finger) and analytically by $N(L)$ poles which are aligned on one line parallel to the imaginary axis. The existence of this solution is made clearer with the following remarks.

2. There exists an attraction between the poles along the real line. The resulting dynamics merges all the x positions of poles whose y-position remains finite.

3. The y positions are distinct, and the poles are aligned above each other in positions $y_{j-1} < y_j < y_{j+1}$ with the maximal being $y_{N(L)}$. This can be understood from equations for the poles motion in which the interaction is seen to be repulsive at short ranges, but changes sign at longer ranges.

4. If one adds an additional pole to such a solution, this pole (or another) will be pushed to infinity along the imaginary axis. If the system has less than $N(L)$ poles it is unstable to the addition of poles, and any noise will drive the system towards this unique state. The number $N(L)$ is

$$N(L) = \left[\frac{1}{2}\left(\frac{L}{\nu}+1\right)\right] , \tag{1.10}$$

where $\left[\ldots\right]$ is the integer part and $2\pi L$ is a system size. To see this consider a system with N poles and such that all the values of y_j satisfy the condition $0 < y_j < y_{max}$. Add now one additional pole whose coordinates are $z_a \equiv (x_a, y_a)$ with $y_a \gg y_{max}$. From the equation of motion for y_a, we see that the terms in the sum are all of the order of unity as is also the $\cot(y_a)$ term. Thus the equation of motion of y_a is approximately

$$\frac{dy_a}{dt} \approx \nu\frac{2N+1}{L^2} - \frac{1}{L} . \tag{1.11}$$

The fate of this pole depends on the number of other poles. If N is too large the pole will run to infinity, whereas if N is small the pole will be attracted towards the real axis. The condition for moving away to infinity is that $N > N(L)$ where $N(L)$ is given by (1.10). On the other hand the y coordinate of the poles cannot hit zero. Zero is a repulsive line, and poles are pushed away from zero with infinite velocity. To see this consider a pole whose y_j approaches zero. For any finite L the term $\coth(y_j)$ grows unboundedly whereas all the other terms in the equation for the poles motion remain bounded.

5. The height of the cusp is proportional to L. The distribution of positions of the poles along the line of constant x was worked out in [12].

We will refer to the solution with all these properties as the Thual-Frisch-Henon (TFH)-cusp solution.

The main results of our own work are as follow. Traditional linear analysis was made for this giant cusp solution. This analysis demonstrates the existence of negative eigenvalues that go to zero when the system size goes to infinity.

1. There exists an obvious Goldstone or translational mode with eigenvalue $\lambda_0 = 0$. This eigenmode stems from the Galilean invariance of the equation of motion.

2. The rescaled eigenvalues ($L^2\lambda_i$) oscillate periodically between values that are L-independent in this presentation. In other words, up to the oscillatory behavior the eigenvalues depend on L like L^{-2}.

3. The eigenvalues λ_1 and λ_2 hit zero periodically. The functional dependence in this presentation appears almost piecewise linear.

4. The higher eigenvalues also exhibit similar qualitative behaviour, but without reaching zero. We note that the solution becomes marginally stable for every value of L for which the eigenvalues λ_1 and λ_2 hit zero. The L^{-2} dependence of the spectrum indicates that the solution becomes more and more sensitive to noise as L increases.

It was proved that arbitrary initial conditions can be written in the term of poles in the complex plane. Inverse cascade process of giant cusp formation was investigated numerically and analytically. Dependences of the flame front width and mean velocity were found. The next step in investigation of the channel case was the influence of random noise on the pole dynamics. The main effect of the external noise is the appearance of new poles in the minima of the flame front and the merging these poles with the giant cusp. The dependence of the mean flame front velocity on the noise and the system size was found. The velocity is almost independent on the noise until the noise achieves some critical value. In the dependence of the velocity on the system size we see growth of the velocity with some exponent until the velocity achieves some saturation value.

Denoting v as the velocity of the flame front and L the system size:

1. We can see two different regimes of behavior the average velocity v as a function of noise f for fixed system size L. For the noise f smaller then same fixed val ue f_{cr}

$$v \sim f^{\xi} \ . \tag{1.12}$$

   For these values of f this dependence is very weak, and $\xi \approx 0.02$. For large values of f the dependence is much stronger

2. We can see growth of the average velocity v as a function of the system size L. After some values of L we can see saturation of the velocity. For regime $f < f_{cr}$ the growth of the velocity can be written as

$$v \sim L^{\mu}, \quad \mu \approx 0.35 \pm 0.03 \ . \tag{1.13}$$

The dependence of the number of poles in the system and the number of the poles that appear in the system in unit time was investigated numerically as a function of the noise and the system parameters. The life time of a pole was found numerically. Theoretical discussion of the effect of noise on the pole dynamics and mean velocity was made [17].

Pole dynamics can be used also to analyse small perturbation of the flame front and make the full stability analysis of the giant cusp. Two kinds of modes were found. The first one is eigenoscillations of the poles in the giant cusp. The second one is modes connected to the appearance of the new poles in the system. The eigenvalues of these modes were found. The results are in good agreement wit h the traditional stability analysis [18].

The results found for the cannel case can be used to analyse flame front propagation in the radial case [19, 20]. Main feature of this case is a competition between attraction of the poles and expanding of the flame front. So in this case we obtain not only one giant cusp but a set of cusps. New poles that appear in the system because of the noise form these cusps. On the basis of the equation of poles motion we can find connection between acceleration of the flame front and the width of the interface. On the basis of the result for mean velocity in the channel case the acceleration of the flame front can be found. So we obtain full picture of the flame front propagation in the radial case.

The next step in the investigation of the problem is considering Laplacian growth with zero surface tension that also has pole solutions. In the case of Laplacian growth we obtain result that is analogous to the merging of the poles in the channel case of the flame front propagation: all poles coalesce into one pole in the case of periodic boundary condition or

two poles on the boundaries in the case of no-flux boundary conditions. This result can be proved theoretically [21].

In papaers [22–26] self-acceleration without involvement of the external forcing is considered. No self-acceleration exist for the finite number of poles. So we can explain the self-acceleration and the appearance of new poles or by the noise or by the "rain" of poles from the "cloud" in infinity. Indeed, any given initial condition can be written as a sum of infinite number of poles(Sec. 2.4.1). Let us consider one pole that appears from the "cloud" in infinity. We neglect by the repulse force from the rest of poles in the system and consider only attraction force in Eqs.(4.13) $-\frac{\gamma}{2r_0}$ For r_0 we can write in the case of self-acceleration $r_0(\tau) = (a+\tau)^\beta, r_0(0) = a^\beta, \beta > 1$. So from $\tau = 0$ to $\tau = \infty$ pole comes down a distance $\Delta y = \int_0^\infty \frac{\gamma}{2r_0(\tau)} d\tau = \frac{\gamma}{2}\frac{1}{\beta-1}\frac{1}{r_0(0)^{\frac{\beta-1}{\beta}}}$. So the "rain" come down the finite distance after the infinite time and this distance converges to zero if $r_0(0) \mapsto \infty$! So we think that the appearance of new poles from the infinity can be explained only by the external noise. The characteristic size of cusp in the system $\mathcal{L} \sim r_0^{\frac{1}{\beta}}$. So from Fig 2.23 the noise $f \sim \frac{1}{\mathcal{L}^5} \sim \frac{1}{r_0^{\frac{5}{\beta}}}$ is necessary for the appearance of new cusps in the system. If the noise is larger than this value the dependence on the noise is very slow($f^0.2$ for regime II and $f^0.02$ for regime III). This result explains the weak dependence of numerical simulations on the noise reduction ([22], Fig.2).

Joulin et al. [27–30] use a vary similar approach for the channel and radial flame growth. But the main attention in our work is made to the velocity of flame front (self-acceleration for the radial case) and the flame front width. Main attention in the channel case in Joulin's work was made to the investigation of mean-spacing between cusps (crests). For the radial case only the linear dependence of radius on time (no self-acceleration) is considered in Joulin's work. Our works greatly complement each other but don't compete with each other.For example, for the distance between cusps (the mean value of cusp) without any proof we use Eq.(2.70). Fig.9([28]) give us a excellent proof of this equation.

The structure of this Thesis is as follow. Chapter 1 is this Introduction.

In Chapter 2 we obtain main results for the channel case of the flame front propagation. We give results about steady state solutions, present traditional linear analysis of the problem and investigate analytically and numerically the influence of noise on the mean velocity of the front and pole dynamics.

In Chapter 3 we obtain results of the linear stability analysis by the help of pole solutions.

In Chapter 4 we use the result obtained for the channel case for analysis of the flame front propagation in the radial case

In Chapter 5 we investigate asymptotic behavior of the poles in the complex plane for the Laplacian growth with the zero surface-tension in the case of periodic and no-flux boundary condition.

Chapter 6 is a summary.

Chapter 2

Pole-Dynamics in Unstable Front Propagation: the Case of the Channel Geometry

2.1 Introduction

The aim of this chapter is to examine the role of random fluctuations on the dynamics of growing wrinkled interfaces which are governed by non-linear equations of motion. We are interested in those examples for which the growth of a flat or smooth interface are inherently unstable. A famous example of such growth phenomena is provided by Laplacian growth patterns [1–3]. The experimental realization of such patterns is seen for example in Hele-Shaw cells [1] in which air or another low viscosity fluid is displacing oil or some other high viscosity fluid. Under normal conditions the advancing fronts do not remain flat; in channel geometries they form in time a stable finger whose width is determined by delicate effects that arise from the existence of surface tension. In radial geometry, the growth the interface forms a contorted and ramified fractal shape. A related phenomenon has been studied in a model equation for flame propagation which has the same linear stability properties as the Laplacian growth problem [9]. The physical problem in this case is that of pre-mixed flames which exist as self-sustaining fronts of exothermic chemical reactions in gaseous combustion. Experiments [10] on flame propagation in radial geometry show that the flame front accelerates as time goes on, and roughens with characteristic exponents. Both observations did not receive proper theoretical explanations. It is notable that the channel and radial growth are markedly different; the former leads to a single giant cusp in the moving front, whereas the latter exhibits infinitely many cusps that appear in a complex hierarchy as the flame front develops ([11, 19] and chapter 4).

Analytic techniques to study such processes are available [38]. In the context of flame propagation [12,15,19,39], and in Laplacian growth in the zero surface-tension limit [6,35,36] one can examine solutions that are described in terms of poles in the complex plane. This description is very useful in providing a set of ordinary differential equations for the positions of the poles, from which one can deduce the geometry of the developing front in an extremely economical and efficient way. Unfortunately this description is not available in the case of Laplacian growth with surface tension, and this makes the flame propagation problem very

attractive. However, it suffers from one fundamental drawback. For the noiseless equation the pole-dynamics always conserves the number of poles that existed in the initial conditions. As a result there is a final degree of ramification that is afforded by every set of initial conditions even in the radial geometry, and it is not obvious how to describe the continuing self-similar growth that is seen in experimental conditions or numerical simulations. Furthermore, as mentioned before, at least in the case of flame propagation one observes [10] an *acceleration* of the flame front with time. Such a phenomenon is impossible when the number of poles is conserved. It is therefore tempting to conjecture that noise may have an important role in affecting the actual growth phenomena that are observed in such systems. In fact, the effect of noise on unstable front dynamics has not been adequately addressed in the literature. From the point of view of analytic techniques noise can certainly generate new poles even if the initial conditions had a finite number of poles. The subject of pole dynamics with the existence of random noise, and the interaction between random fluctuations and deterministic front propagation are the main issues of this chapter.

We opt to study the example of flame propagation rather than Laplacian growth, simply because the former has an analytic description in terms of poles also in the experimentally relevant case of finite viscosity. We choose to begin the study with channel geometry. The reason is that in radial geometry it is more difficult to disentangle the effects of external noise from those of initial conditions. After all, initially the system can contain infinitely many poles,very far away near infinity in the complex plane (and therefore having an infinitely small contribution to the interface). Since the growth of the radius changes the stability of the system, more and more of these poles might fall down to the real axis and become observable. In channel geometry the analysis of the effect of initial conditions is relatively straightforward, and one can understand it before focusing on the (more interesting) effects of external noise [12]. The basic reason for this is that in this geometry the noiseless steady state solution for the developed front is known analytically. As described in Section II, in a channel of width L the steady-state solution is given in terms of $N(L)$ poles that are organized on a line parallel to the imaginary axis. It can be shown that for any number of poles in the initial conditions this is the only attractor of the pole dynamics. After the establishment of this steady state we can begin to systematically examine the effects of external noise on this solution. As stated before, in radial conditions there is no stable steady state with a finite number of poles, and the disentanglement of initial vs. external perturbations is less straightforward ([19] and chapter 4). We show later that the insights provided in this chapter have relevance for radial growth as well as will be discussed in the sequel.

We have a number of goals in this chapter. Firstly, after introducing the pole decomposition, the pole dynamics, and the basic steady state, we will present stability analysis of the solutions of the flame propagation problem in a channel geometry. It will be shown that the giant cusp solution is linearly stable, but non-linearly unstable. These results, which are described in Section III, can be obtained either by linearizing the dynamics around the giant cusp solutions in order to study the stability eigenvalues, or by examining perturbations in the form of poles in the complex plane. The main result of Section III is that there exists one Goldstone mode and two modes whose eigenvalues hit the real axis periodically when the system size L increases. Thus the system is marginally stable at particular values of L, and it is always nonlinearly unstable, allowing finite size perturbations to introduce new poles into the system. This insight allows us to understand the relation between the system size and the effects of noise. In Section IV we discuss the relaxation dynamics that ensues

after starting the system with "small" initial data. We study the coarsening process that leads in time to the final solution of the giant cusp, and understand from this what are the typical time scales that exist in our dynamics. We offer in this Section some results of numerical simulations that are interpreted in the later sections. In Section V we focus on the phenomenon of acceleration of the flame front and its relation to the existence of noise. In noiseless conditions the velocity of the flame front in a finite channel is bounded [12]. This can be shown either by using the pole dynamics or directly from the equation of motion. We will present the results of numerical simulations where the noise is controlled, and show how the velocity of the flame front is affected by the level of the noise and the system size. The main results are: (i) Noise is responsible for introducing new poles to the system; (ii) For low levels of noise the velocity of the flame front scales with the system size with a characteristic exponent; (iii) There is a phase transition at a sharp (but system-size dependent) value of the noise-level, after which the behavior of the system changes qualitatively; (iv) After the phase transition the velocity of the flame front changes very rapidly with the noise level. In the last Section we remark on the implications of these observations for the scaling behavior of the radial growth problem, and present a summary and conclusions.

2.2 Equations of Motion and Pole-decomposition in the Channel Geometry

It is known that planar flames freely propagating through initially motionless homogeneous combustible mixtures are intrinsically unstable. It was reported that such flames develop characteristic structures which include cusps, and that under usual experimental conditions the flame front accelerates as time goes on. A model in $1+1$ dimensions that pertains to the propagation of flame fronts in channels of width $\tilde{L}$ was proposed in [9]. It is written in terms of position $h(x,t)$ of the flame front above the x-axis. After appropriate rescalings it takes the form:

$$\frac{\partial h(x,t)}{\partial t} = \frac{1}{2}\left[\frac{\partial h(x,t)}{\partial x}\right]^2 + \nu\frac{\partial^2 h(x,t)}{\partial x^2} + I\{h(x,t)\} + 1 \ . \tag{2.1}$$

The domain is $0 < x < \tilde{L}$, ν is a parameter and we use periodic boundary conditions. The functional $I[h(x,t)]$ is the Hilbert transform which is conveniently defined in terms of the spatial Fourier transform

$$h(x,t) = \int_{-\infty}^{\infty} e^{ikx}\hat{h}(k,t)dk \tag{2.2}$$

$$I[h(k,t)] = |k|\hat{h}(k,t) \tag{2.3}$$

For the purpose of introducing the pole-decomposition it is convenient to rescale the domain to $0 < \theta < 2\pi$. Performing this rescaling and denoting the resulting quantities with the same notation we have

$$\frac{\partial h(\theta,t)}{\partial t} = \frac{1}{2L^2}\left[\frac{\partial h(\theta,t)}{\partial \theta}\right]^2 + \frac{\nu}{L^2}\frac{\partial^2 h(\theta,t)}{\partial \theta^2}$$
$$+\frac{1}{L}I\{h(\theta,t)\} + 1 \ . \tag{2.4}$$

In this equation $L = \tilde{L}/2\pi$. Next we change variables to $u(\theta,t) \equiv \partial h(\theta,t)/\partial\theta$. We find

$$\frac{\partial u(\theta,t)}{\partial t} = \frac{u(\theta,t)}{L^2}\frac{\partial u(\theta,t)}{\partial \theta} + \frac{\nu}{L^2}\frac{\partial^2 u(\theta,t)}{\partial \theta^2} + \frac{1}{L} I\{u(\theta,t)\} \ . \tag{2.5}$$

It is well known that the flat front solution of this equation is linearly unstable. The linear spectrum in k-representation is

$$\omega_k = |k|/L - \nu k^2/L^2 \ . \tag{2.6}$$

There exists a typical scale k_{max} which is the last unstable mode

$$k_{max} = \frac{L}{\nu} \ . \tag{2.7}$$

Nonlinear effects stabilize a new steady-state which is discussed next.

The outstanding feature of the solutions of this equation is the appearance of cusp-like structures in the developing fronts. Therefore a representation in terms of Fourier modes is very inefficient. Rather, it appears very worthwhile to represent such solutions in terms of sums of functions of poles in the complex plane. It will be shown below that the position of the cusp along the front is determined by the real coordinate of the pole, whereas the height of the cusp is in correspondence with the imaginary coordinate. Moreover, it will be seen that the dynamics of the developing front can be usefully described in terms of the dynamics of the poles. Following [12,19,38,39] we expand the solutions $u(\theta,t)$ in functions that depend on N poles whose position $z_j(t) \equiv x_j(t) + iy_j(t)$ in the complex plane is time dependent:

$$\begin{aligned} u(\theta,t) &= \nu \sum_{j=1}^{N} \cot\left[\frac{\theta - z_j(t)}{2}\right] + c.c. \\ &= \nu \sum_{j=1}^{N} \frac{2\sin[\theta - x_j(t)]}{\cosh[y_j(t)] - \cos[\theta - x_j(t)]} \ , \end{aligned} \tag{2.8}$$

$$h(\theta,t) = 2\nu \sum_{j=1}^{N} \ln\Big[\cosh(y_j(t)) - \cos(\theta - x_j(t))\Big] + C(t) \ . \tag{2.9}$$

In (2.9) $C(t)$ is a function of time. The function (2.9) is a superposition of quasi-cusps (i.e. cusps that are rounded at the tip). The real part of the pole position (i.e. x_j) is the coordinate (in the domain $[0, 2\pi]$) of the maximum of the quasi-cusp, and the imaginary part of the pole position (i.e y_j) is related to the depth of the quasi-cusp. As y_j decreases the depth of the cusp increases. As $y_j \to 0$ the depth diverges to infinity. Conversely, when $y_j \to \infty$ the depth decreases to zero.

The main advantage of this representation is that the propagation and wrinkling of the front can be described via the dynamics of the poles. Substituting (2.8) in (2.5) we derive the following ordinary differential equations for the positions of the poles:

$$-L^2 \frac{dz_j}{dt} = \Big[\nu \sum_{k=1,k\neq j}^{2N} \cot\left(\frac{z_j - z_k}{2}\right) + i\frac{L}{2} sign[Im(z_j)]\Big]. \tag{2.10}$$

We note that in (2.8), due to the complex conjugation, we have $2N$ poles which are arranged in pairs such that for $j < N$ $z_{j+N} = \bar{z}_j$. In the second sum in (2.8) each pair of poles contributed one term. In Eq.(2.10) we again employ $2N$ poles since all of them interact. We can write the pole dynamics in terms of the real and imaginary parts x_j and y_j. Because of the arrangement in pairs it is sufficient to write the equation for either $y_j > 0$ or for $y_j < 0$. We opt for the first. The equations for the positions of the poles read

$$-L^2\frac{dx_j}{dt} = \nu \sum_{k=1,k\neq j}^{N} \sin(x_j - x_k)\Big[[\cosh(y_j - y_k) \tag{2.11}$$
$$-\cos(x_j - x_k)]^{-1} + [\cosh(y_j + y_k) - \cos(x_j - x_k)]^{-1}\Big]$$
$$L^2\frac{dy_j}{dt} = \nu \sum_{k=1,k\neq j}^{N} \Big(\frac{\sinh(y_j - y_k)}{\cosh(y_j - y_k) - \cos(x_j - x_k)}$$
$$+\frac{\sinh(y_j + y_k)}{\cosh(y_j + y_k) - \cos(x_j - x_k)}\Big) + \nu\coth(y_j) - L. \tag{2.12}$$

We note that if the initial conditions of the differential equation (2.5) are expandable in a finite number of poles, these equations of motion preserve this number as a function of time. On the other hand, this may be an unstable situation for the partial differential equation, and noise can change the number of poles. This issue will be examined at length in Section 2.5.

2.3 Linear Stability Analysis in Channel Geometry

In this section we discuss the linear stability of the TFH-cusp solution. To this aim we first use Eq.(2.8) to write the steady solution $u_s(\theta)$ in the form:

$$u_s(\theta) = \nu\sum_{j=1}^{N} \frac{2\sin[\theta - x_s]}{\cosh[y_j] - \cos[\theta - x_s]}\ , \tag{2.13}$$

where x_s is the real (common) position of the stationary poles and y_j their stationary imaginary position. To study the stability of this solution we need to determine the actual positions y_j. This is done numerically by integrating the equations of motion for the poles starting from N poles in initial positions and waiting for relaxation. Next one perturbs this solution with a small perturbation $\phi(\theta, t)$: $u(\theta, t) = u_s(\theta) + \phi(\theta, t)$. Linearizing the dynamics for small ϕ results in the equation of motion

$$\frac{\partial\phi(\theta,t)}{\partial t} = \frac{1}{L^2}\Big[\partial_\theta[u_s(\theta)\phi(\theta,t)] + \nu\partial_\theta^2\phi(\theta,t)\Big]$$
$$+\frac{1}{L}I(\phi(\theta,t))\ . \tag{2.14}$$

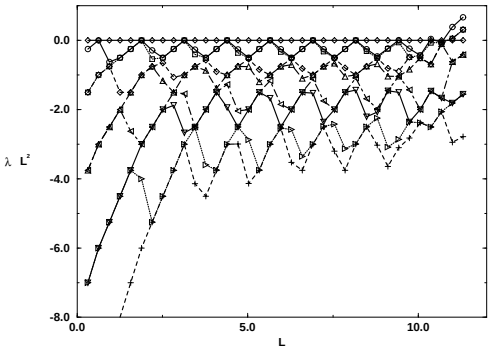

Figure 2.1: The first 10 highest eigenvalues of the stability matrix with $\nu = \pi/5$, multiplied by the square of the system size L^2 vs. the system size L. Note that all the eigennvalues oscillate around fixed values in this presentation, and that the highest two eigenvalues hit zero periodically.

2.3.1 Fourier decomposition and eigenvalues

The linear equation can be decomposed in Fourier modes according to

$$\phi(\theta,t) = \sum_{k=-\infty}^{\infty} \hat{\phi}_k(t) e^{ik\theta} \tag{2.15}$$

$$u_s(\theta) = -2\nu i \sum_{k=-\infty}^{\infty} \sum_{j=1}^{N} \mathrm{sign}(k) e^{-|k|y_j} e^{ik\theta} \tag{2.16}$$

In these sums the discrete k values run over all the integers. Substituting in (2.14) we get the equations:

$$\frac{d\hat{\phi}_k(t))}{dt} = \sum_n a_{kn} \hat{\phi}_n(t) \ , \tag{2.17}$$

where a_{kn} is a infinite matrix whose entries are given by

$$a_{kk} = \frac{\mid k \mid}{L} - \frac{\nu}{L^2} k^2 \tag{2.18}$$

$$a_{kn} = \frac{k}{L^2} \mathrm{sign}(k-n)(2\nu \sum_{j=1}^{N} e^{-|k-n|y_j}) \quad k \neq n \ . \tag{2.19}$$

To solve for the eigenvalues of this matrix we need to truncate it at some cutoff k-vector k^*. The choice of k^* can be based on the linear stability analysis of the flat front. The scale k_{max}, cf. (2.7), is the largest k which is still linearly unstable. We must choose $k^* > k_{max}$ and test the choice by the converegence of the eigenvalues. The chosen value of k^* in our numerics was $4k_{max}$. The results for the low order eigenvalues of the matrix a_{kn} that were obtained from a converged numerical calculation are presented in Fig.2.1.

The eigenvalues are multiplied by L^2 and are plotted as a function of L. We order the eigenvalues in decreasing order and denote them as $\mid \lambda_0 \mid \leq \mid \lambda_1 \mid \leq \mid \lambda_2 \mid \ldots$.

Fig 2.1 contains a strange result on the positive eigenvalues at large L. One of methods to check some numerical result is to do analytic investigation. For example, in Chapter 3 we make detailed analytic investigation for the numerical result on Fig. 2.1 and obtain that all eigenvalues are not positive. Indeed, two types of modes exists. The first one is connected to the displacement of poles in the giant cusp. Because of the pole attraction the giant cusp is stable with respect to the longitudinal displacement of poles and so the correspondent eigenvalues are not positive. For the transversal displacement the Lyapunov function exists and so the giant cusp is stable with respect to the transversal displacement and the correspondent eigenvalues are not positive. The second type of modes is connected to additional poles. These poles go to infinity because of the repulsion from the giant cusp poles $N(L)$. So the correspondent eigenvalues are also not positive. So the positive eigenvalues at large L are a numerical artifact.

The figure offers a number of qualitative observations:

1. There exists an obvious Goldstone or translational mode $u_s'(\theta)$ with eigenvalue $\lambda_0 = 0$, which is shown with rhombes in Fig.2.1. This eigenmode stems from the Galilean invariance of the equation of motion.

2. The eigenvalues oscillate periodically between values that are L-independent in this presentation (in which we multiply by L^2). In other words, up to the oscillatory behavior the eigenvalues depend on L like L^{-2}.

3. The eigenvalues λ_1 and λ_2, which are represented by squares and circles in Fig.2.1, hit zero periodically. The functional dependence in this presentation appears almost piecewise linear.

4. The higher eigenvalues also exhibit similar qualitative behaviour, but without reaching zero. We note that the solution becomes marginally stable for every value of L for which the eigenvalues λ_1 and λ_2 hit zero. The L^{-2} dependence of the spectrum indicates that the solution becomes more and more sensitive to noise as L increases.

2.3.2 Qualitative understanding using pole-analysis

The most interesting qualitative aspects are those enumerated above as item 2 and 3. To understand them it is useful to return to the pole description, and to focus on Eq.(1.11). This equation describes the dynamics of a single far-away pole. We remarked before that this equation shows that for *fixed* L the stable number of poles is the integer part (1.10). Define now the number α, $0 \leq \alpha \leq 1$, according to

$$\alpha = \left[\frac{1}{2}\left(\frac{L}{\nu} + 1\right)\right] - \frac{1}{2}\left(\frac{L}{\nu} - 1\right) \ . \tag{2.20}$$

Using this number we rewrite Eq.(1.11) as

$$\frac{dy_a}{dt} \approx \frac{2\nu}{L^2}\alpha \ . \tag{2.21}$$

As L increases, α oscillates piecewise linearly and periodically between zero and unity. This shows that a distant pole which is added to the giant cusp solution is usually repelled to

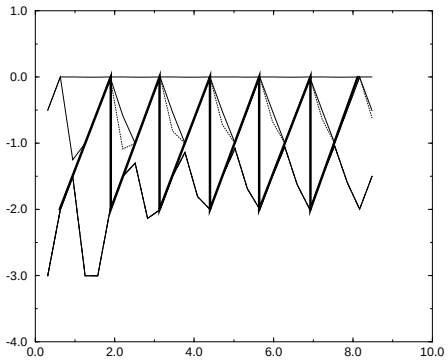

Figure 2.2: Comparison of the numerically determined highest 4 eigenvalues of the stability matrix with the prediction of the pole analysis. The eigenvalues of the stabilit y matrix are :λ_0, λ_1, λ_2 and λ_3. The pole analysis (solid line) provides a qualitative understanding of the stability, and appears to overlap with the high est eigenvector over half of the range, and with the fourth eigenvalue over the other half.

infinity except when α hits zero and the system becomes marginally unstable to the addition of a new pole.

To connect this to the linear stability analysis we note from Eq.(2.8) that a single far-away pole solution (i.e with y very large) can be written as

$$u(\theta, t) = 4\nu e^{-y(t)} \sin(\theta - x(t)) \ . \tag{2.22}$$

Suppose that we add to our giant cusp solution a perturbation of this functional form. ¿From Eq.(2.21) we know that y grows linearly in time, and therefore this solution decays exponentially in time. The rate of decay is a linear eigenvalue of the stability problem, and from Eq.(2.21) we understand both the $1/L^2$ dependence and the periodic marginality. We should note that this way of thinking gives us a significant part of the L dependence of the eigenvalues, but not all. The variable α is rising from zero to unity periodically, but after reaching unity it hits zero instantly. Accordingly, if the highest non zero eigenvalue were fully determined by the pole analysis, we would expect this eigenvalue to behave as the solid line shown in Fig.2.2.

The actual highest eigenvalue computed from the stability matrix is shown in rhombes connected by dotted line. It is clear that the pole analysis gives us a great deal of qualitative and quantitative understanding, but not all the features agree.

2.3.3 Dynamics near marginality

The discovery of marginality at isolated values of L poses questions regarding the fate of poles that are added at very large y's at certain x-positions. We will argue now that when the system becomes marginally stable, a new pole can be added to those existing in the giant cusp. We remember that these poles have a common θ position that we denote as $\theta = \theta_c$. The fate of a new pole added at infinity depends on its θ position. If the position of the new

pole is again denoted as y_a, and $\infty \gg y_a \gg y_{max}$, we can see from Eq.(2.12) that dy_a/dt is maximal when $\theta_a = \theta_c$, whereasit is minimal when $\theta_a - \theta_c = \pi$. This follows from the fact that the cosine term has a value $+1$ when $\theta_a = \theta_c$ and a value -1 when $\theta_a - \theta_c = \pi$. For large y differences the terms in the sum take on their minimal value when the cos term is -1 and their maximal values at $+1$. For infinitely large y_a the equation of motion is (1.11) which is independent of θ_a. Since the RHS of this equation becomes zero at marginality, we conclude that for very large but finite y_a dy_a/dt changes sign from positive to negative when $\theta_a - \theta_c$ changes from zero to π. The meaning of this observation is that the most unstable points in the system are those points which are furthest away from the giant cusp. It is interesting to discuss the fate of a pole that is added to the system at such a position. From the point of view of the pole dynamics $\theta = \theta_c + \pi$ is an unstable fixed point for the motion along the θ axis. The attraction to the giant cusp exactly vanishes at this point. If we start with a pole at a very large y_a close to this value of θ the down-fall along the y coordinate will be faster than the lateral motion towards the giant cusp. We expect to see therefore the creation of a small cusp at θ values close to π that precedes a later stage of motion in which the small cusp moves to merge with the giant cusp. Upon the approach of the new pole to the giant cusp all the existing poles will move up and the furthest pole at y_{max} will be kicked off to infinity. We will later explain that this type of dynamics occurs in stable systems that are driven by noise. The noise generates far away poles (in the imaginary direction) that get attracted around $\theta = \theta_c + \pi$ to create small cusps that run continuously towards the giant cusp.

2.3.4 Excitable System.

The intuition gained so far can be used to discuss the issue of stability of a stable system to *larger* perturbations. In other words, we may want to add to the system poles at finite values of y and ask about their fate. We first show in this subsection that poles whose initial y value is below $y_{max} \sim \log(L^2/\nu^2)$ will be attracted towards the real axis. The scenario is similar to the one described in the last paragraph.

Suppose that we generate a stable system with a giant cusp at $\theta_c = 0$ with poles distributed along the y axis up to y_{max}. We know that the sum of all the forces that act on the upper pole is zero. Consider then an additional pole inserted in the position (π, y_{max}). It is obvious from Eq.(2.12) that the forces acting on this pole will pull it downward. On the other hand if its initial position is much above y_{max} the force on it will be repulsive towards infinity. We see that this simple argument identifies y_{max} as the typical scale for nonlinear instability.

Next we estimate y_{max} and interpret our result in terms of the *amplitude* of a perturbation of the flame front. We explained that uppermost pole's position fluctuates between a minimal value and infinity as L is changing. We want to estimate the characteristic scale of the minimal value of $y_{max}(L)$. To this aim we employ the result of ref. [12] regarding the stable distribution of pole positions in a stable large system. The parametrization of [12] differs from ours; to go from our parametrization in Eq.(2.5) to theirs we need to rescale u by L^{-1} and t by L. The parameter ν in their parameterization is ν/L in ours. According to [12] the number of poles between y and $y + dy$ is given by the $\rho(y)dy$ where the density $\rho(y)$ is

$$\rho(y) = \frac{L}{\pi^2 \nu} \ln[\coth(|y|/4)] \ . \tag{2.23}$$

To estimate the minimal value of y_{max} we require that the tail of the distribution $\rho(y)$ integrated between this value and infinity will allow one single pole. In other words,

$$\int_{y_{max}}^{\infty} dy\rho(y) \approx 1 \ . \tag{2.24}$$

Expanding (2.23) for large y and integrating explicitly the result in (2.24) we end up with the estimate

$$y_{max} \approx 2 \ln \Big[\frac{4L}{\pi^2 \nu}\Big] \tag{2.25}$$

For large L this result is $y_{max} \approx \ln(\frac{L^2}{\nu^2})$. If we now add an additional pole in the position (θ, y_{max}) this is equivalent to perturbing the solution $u(\theta, t)$ with a function $\nu e^{-y_{max}} \sin(\theta)$, as can be seen directly from (2.8). We thus conclude that the system is unstable to a perturbation *larger* than

$$u(\theta) \sim \nu^3 \sin(\theta)/L^2 \ . \tag{2.26}$$

This indicates a very strong size dependence of the sensitivity of the giant cusp solution to external perturbations. This will be an important ingredient in our discussion of noisy systems.

2.4 Initial Conditions, Pole Decomposition and Coarsening

In this section we show first that any initial conditions can be approximated by pole decomposition. Later, we show that the dynamics of sufficiently smooth initial data can be well understood from the pole decomposition. Finally we employ this picture to describe the *inverse cascade* of cusps into the giant cusp which is the final steady state. By inverse cascade we mean a nonlinear coarsening process in which the small scales coalesce in favor of larger scales and finally the system staturates at the largest available scale [40].

2.4.1 Pole Expansion: General Comments

The fundamental question is how many poles are needed to describe any given initial condition. The answer, of course, depends on how smooth are the initial conditions. Suppose also that we have an initial function $u(\theta, t = 0)$ that is 2π-periodic and which at time $t = 0$ admits a Fourier representation

$$u(\theta) = \sum_{k=1}^{\infty} A_k \sin\left(k\theta + \phi_k\right) \ , \tag{2.27}$$

with $A_k > 0$ for all k. Suppose that we want to find a pole-decomposition representation $u_p(\theta)$ such that

$$|u_p(\theta) - u(\theta)| \leq \epsilon \qquad \text{for every} \quad \theta \ , \tag{2.28}$$

where ϵ is a given wanted accuracy. If $u(\theta)$ is differentiable we can cut the Fourier expansion at some finite $k = K$ knowing that the remainder is smaller than, say, $\epsilon/2$. Choose now a

large number M and a small number $\Delta \ll 1/M$ and write the pole representation for $u_p(\theta)$ as

$$u_p(\theta) = \sum_{k=1}^{K} \sum_{p=0}^{M-1} \frac{2k \sin(k\theta + \phi_k)}{\cosh[k(y_k + p\Delta)] - cos(k\theta + \phi_k)} \ . \tag{2.29}$$

To see that this representation is a particular form of the general formula (2.8) We use the following two identities

$$\sum_{k=0}^{\infty} e^{-kt} \sin xk = \frac{1}{2} \frac{\sin x}{\cosh t - \cos x} \ , \tag{2.30}$$

$$\sum_{k=0}^{K-1} \sin(x + ky) = \sin(x + \frac{K-1}{2} y) \sin \frac{Ky}{2} \mathrm{cosec} \frac{y}{2} \ . \tag{2.31}$$

From these follows a third identity

$$\begin{aligned} &\sum_{j=0}^{K-1} \frac{2 \sin(x - \frac{2\pi j}{K} + \phi)}{\cosh y - \cos(x - \frac{2\pi j}{K} + \phi)} \\ &= \frac{2K \sin(Kx + \phi)}{\cosh Ky - \cos(Kx + \phi)} \ . \end{aligned} \tag{2.32}$$

Note that the LHS of (2.32) is of the form (2.8) with K poles whose positions are all on the line $y_j = y$ and whose x_j are on the lattice points $2\pi j/K - \phi$. On the other hand every term in (2.29) is of this form.

Next we use (2.30) to rewrite (2.29) in the form

$$u_p(\theta) = \sum_{k=1}^{K} \sum_{p=0}^{M-1} \sum_{n=1}^{\infty} 4k e^{-nk(y_k + p\Delta)} \sin(nk\theta + n\phi_k) \ . \tag{2.33}$$

Exchanging order of summation between n and p we can perform the geometric sum on p. Denoting

$$b_{n,k} \equiv \sum_{p=0}^{M-1} e^{-nkp\Delta} = \frac{1 - e^{-Mkn\Delta}}{1 - e^{-kn\Delta}} \ , \tag{2.34}$$

we find

$$\begin{aligned} u_p(\theta) &= \sum_{k=1}^{K} \sum_{n=1}^{\infty} 4k b_{n,k} e^{-nky_k} \sin(nk\theta + n\phi_k) \\ &= \sum_{k=1}^{K} \sum_{n=2}^{\infty} 4k b_{n,k} e^{-nky_k} \sin(nk\theta + n\phi_k) \\ &+ \sum_{k=1}^{K} 4k b_{1,k} e^{-ky_k} \sin(k\theta + \phi_k) \ . \end{aligned} \tag{2.35}$$

Compare now the second term on the RHS of (2.35) with (2.27). We can identify

$$e^{-ky_k} = \frac{A_k}{4k b_{1,k}} \tag{2.36}$$

The first term can be then bound from above as

$$\Big|\sum_{k=1}^{K}\sum_{n=2}^{\infty} 4kb_{n,k}e^{-nky_k}\sin\left(nk\theta+n\phi_k\right)\Big| \tag{2.37}$$
$$\leq \sum_{k=1}^{K}\sum_{n=2}^{\infty}\Big|4kb_{n,k}\left[\frac{A_k}{4kb_{1,k}}\right]^n\sin\left(nk\theta+n\phi_k\right)\Big|.$$

The sine function and the factor $(4K)^{1-n}$ can be replaced by unity and we can bound the RHS of (2.37) by

$$\sum_{k=1}^{K}\sum_{n=2}^{\infty}\left[\frac{A_k}{b_{1,k}}\right]^n b_{n,k} \leq \sum_{k=1}^{K} A_k \sum_{n=1}^{\infty}\left[\frac{A_k}{b_{1,k}}\right]^n, \tag{2.38}$$

where we have used the fact that $b_{n,k} \leq b_{1,k}$ which follows directly from (2.34). Using now the facts that $b_{1,K} \leq b_{1,k}$ for every $k \leq K$ and that A_k is bounded by some finite C since it is a Fourier coefficient, we can bound (2.38) by $C^2K/(b_{1,K}-C)$. Since we can select the free parameters Δ and M to make $b_{1,K}$ as large as we want, we can make the remainder series smaller in absolute value than $\epsilon/2$.

The conclusion of this demonstration is that any initial condition that can be represented in Fourier series can be approximated to a desired accuracy by pole-decomposition. The number of needed poles is of the order $K^2 \times M$. Of course, the number of poles thus generated by the initial conditions may exceed the number $N(L)$ found in Eq.(1.10). In such a case the excess poles will move to infinity and will become irrelevant for the short time dynamics. Thus a smaller number of poles may be needed to describe the state at larger times than at $t = 0$. We need to stress at this point that the pole decomposition is over complete; for example, if there is exactly one pole at $t = 0$ and we use the above technique to reach a pole decomposition we would get a large number of poles in our representation.

2.4.2 The initial stages of the front evolution: the exponential stage and the inverse cascade

In this section we employ the connection between Fourier expansion and pole decomposition to understand the initial exponential stage of the evolution of the flame front with small initial data $u(\theta, t = 0)$. Next we employ our knowledge of the pole interactions to explain the slow dynamics of coarsening into the steady state solution.

Suppose that initially the expansion (2.27) is available with all the coefficients $A_k \ll 1$. We know from the linear instability of the flat flame front that each Fourier component changes exponentially in time according to the linear spectrum (2.6). The components with wave vector larger than (2.7) decrease, whereas those with lower wave vectors increase. The fastest growing mode is $k_c = L/2\nu$. In the linear stage of growth this mode will dominate the shape of the flame front, i.e.

$$u(\theta, t) \approx A_{k_c}e^{\omega_{k_c}t}\sin(k_c\theta)\ . \tag{2.39}$$

Using Eq.(2.32) for a large value of y (which is equivalent to small A_{k_c}) we see that to the order of $O(A_{k_c}^2)$ (2.39) can be represented as a sum over $L/2\nu$ poles arranged periodically along the θ axis. Other unstable modes will contribute similar arrays of poles but at much higher

values of y, since their amplitude is exponentially smaller. In addition we have nonlinear corrections to the identification of the modes in terms of poles. These corrections can be again expanded in terms of Fourier modes, and again identified with poles, which will be further away along the y axis, and with higher frequencies. To see this one can use Eq.(2.35), subtract from $u_p(\theta)$ the leading pole representations, and reexpand in Fourier series. Then we identify the leading order with double the number of poles that are situated twice further away along the y axis.

We note that even when all the unstable modes are present, the number of poles in the first order identification is finite for finite L, since there are only L/ν unstable modes. Counting the number of poles that each mode introduces we get a total number of $\left(L/\nu\right)^2$ poles. The number $L/2\nu$ of poles which are associated with the most unstable mode is precisely the number allowed in the stable stationary solution, cf.(1.10). When the poles approach the real axis and cusps begin to develop, the linear analysis no longer holds, but the pole description does.

We now describe the qualitative scenario for the establishment of the steady state. Firstly, we understand that all the poles that belong to less unstable modes will be pushed towards infinity. To see this think of the system at this stage as an array of uncoupled systems with a scale of the order of unity. Each such system will have a characteristic value of y. As we discussed before poles that are further away along the y axis will be pushed to infinity. Therefore the system will remain with the $L/2\nu$ poles of the most unstable mode. The net effect of the poles belonging to the (nonlinearly) stable modes is to destroy the otherwise perfect periodicity of the poles of the unstable mode. The see the effect of the higher order correction to the pole identification we again recall that they can be represented as further away poles with higher frequencies, whose dynamics is similar to the less unstable modes that were just discussed. They do not become more relevant when time goes on.

Once the poles of the stable modes get sufficiently far from the real axis, the dynamics of the remaining poles will begin to develop according to the interactions that are directed along the real axis. These interactions are much weaker and the resulting dynamics occur on much longer time scales. The qualitative picture is of an inverse cascade of merging the θ positions of the poles. We note that the system has a set of unstable fixed points which are 'cellular solutions' described by a periodic arrangement of poles along the real axis with a frequency k. These fixed points are not stable and they collapse, under perturbations, with a characteristic time scale (that depends on k) to the next unstable fixed point at $k' = k/2$. This process then goes on indefinitely until $k \sim 1/L$ i.e. we reach the giant cusp, the steady-state stable solution [40].

This scenario is seen very clearly in the numerical simulations. In Fig.2.3 we show

the time evolution of the flame front starting from small white-noise initial conditions. The bottom curve pertains to the earliest time in this picture, just after the fast exponential growth, and one sees clearly the periodic array of cusps that form. The successive images show the progress of the flame front in time, and one observes the development of larger scales with deeper cusps that represent the partial coalescence of poles onto the same θ positions. In Fig.2.4

we show the width and the velocity of this front as a function of time. One recognizes the exponential stage of growth in which the $L/2\nu$ poles approach the θ axis, and then a clear cross-over to much slower dynamics in which the effective scale in the system grows with a

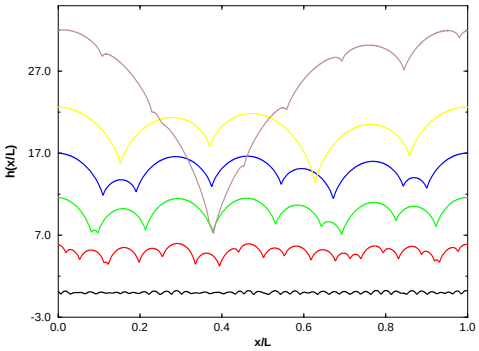

Figure 2.3: The inverse cascade process of coarsening that occurs after preparing the system with random, small initial conditions. One sees that at successive times the typical scale increases until the giant cusp forms, and attracts all the other side-poles. The effect of the existing numerical additive noise is to introduce poles that appear as side cusps that are continuously attracted to the giant cusp. This effect is obvious to the eye only after the typical scale is sufficiently large, as is seen in the last time (see text for further details).

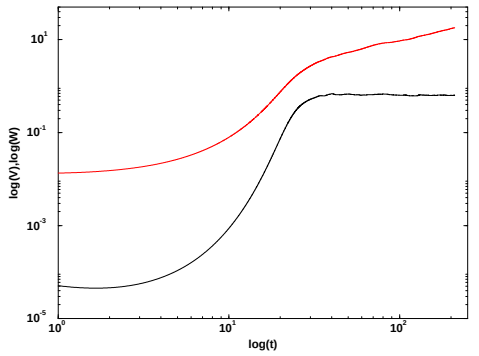

Figure 2.4: log-log plots of the front velocity (lower curve) and width (upper curve) as a function of time in the inverse cascade process seen in Fig.2.3 in a system o f size 2000 and $\nu = 1$. Both quantities exhibit an initial exponential growth that turns to a power law growth (after $t \approx 30$). The velocity is constant after this time, and the width increases like t^{ζ}. Note that at the earliest time there is a slight decrease in the velocity; this is due to the decay of linearly stable modes that exist in random initial conditions.

slower rate.

The slow dynamics stage can be understood qualitatively using the previous interpretation of the cascade as follows: if the initial number of poles belonging to the unstable mode is $L/2\nu$, the initial effective linear scale is 2ν. Thus the first step of the inverse cascade will be completed in a time scale of the order of 2ν. At this point the effective linear scale doubles to 4ν, and the second step will be completed after such a time scale. We want to know what is the typical length scale l_t seen in the system at time t. The definition of front width is $l_t = \sqrt{\frac{1}{\tilde{L}}\int_0^{\tilde{L}}[h(x,t)-\bar{h}]^2 dx}, \bar{h} = \frac{1}{\tilde{L}}\int_0^{\tilde{L}} h(x,t)dx$. The typical width of the system at this stage will be proportional to this scale.

Denote the number of cascade steps that took place until this scale is achieved by s_l. The total time elapsed, $t(l_t)$ is the sum

$$t(l_t) \sim \sum_{i=1}^{s_l} 2^i \ . \tag{2.40}$$

The geometric sum is dominated by the largest term and we therefore estimate $t(l_t) \sim l_t$. We conclude that the scale and the width are linear in the time elapsed from the initial conditions ($l_t \sim t^\zeta,\ \zeta = 1$). In noiseless simulations we find (see Fig.2.4) a value of ζ which is $\zeta \approx 0.95 \pm 0.1$.

2.4.3 Inverse cascade in the presence of noise

An interesting consequence of the discussion in the last section is that the inverse cascade process is an effective "clock" that measures the typical time scales in this system. For future purposes we need to know the typical time scales when the dynamics is perturbed by random noise. To this aim we ran simulations following the inverse cascade in the *presence* of external noise. The main result that will be used in later arguments is that now the appearance of a typical scale l_t occurs not after time t, but rather according to

$$l_t \sim t^\zeta \ , \quad \zeta \approx 1.2 \pm 0.1 \ . \tag{2.41}$$

The numerical confirmation of this law is exhibited in Fig.2.5 .

We also find that the front velocity in this case increases with time according to

$$v \sim t^\gamma \ , \quad \gamma \approx 0.48 \pm 0.05 \ . \tag{2.42}$$

This result will be related to the acceleration of the flame front in noisy simulations, as will be seen in the next Sections.

2.5 Acceleration of the Flame Front, Pole Dynamics and Noise

A major motivation of this Section is the observation that in radial geometry the same equation of motion shows an acceleration of the flame front. The aim of this section is to argue that this phenomenon is caused by the noisy generation of new poles. Moreover, it is our contention that a great deal can be learned about the acceleration in radial geometry by

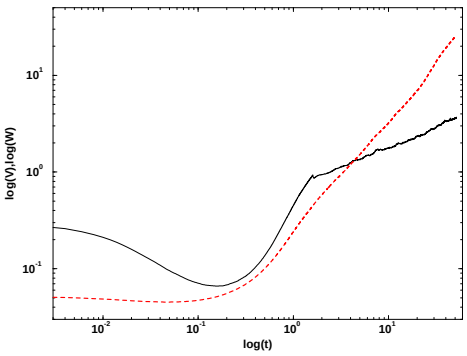

Figure 2.5: The same as Fig.2.4 but with additive random noise for a system of size 1000, $\nu = 0.1$ and $f = 10^{-13}$. The velocity does not saturate now, and the exponent ζ characterizing the increase of the width with time changes to $\zeta = 1.2 \pm 0.1$. The velocity increases in time like t^{γ} with $\gamma \approx 0.48 \pm 0.04$.

considering the effect of noise in channel growth. In Ref. [12] it was shown that any initial condition which is represented in poles goes to a unique stationary state which is the giant cusp which propagates with a constant velocity $v = 1/2$ up to small $1/L$ corrections. In light of our discussion of the last section we expect that any smooth enough initial condition will go to the same stationary state. Thus if there is no noise in the dynamics of a finite channel, no acceleration of the flame front is possible. What happens if we add noise to the system?

For concreteness we introduce an additive white-noise term $\eta(\theta, t)$to the equation of motion (2.5) where

$$\eta(\theta, t) = \sum_k \eta_k(t) \exp(ik\theta) \ , \tag{2.43}$$

and the Fourier amplitudes η_k are correlated according to

$$< \eta_k(t)\eta^*_{k'}(t') >= \frac{f}{L}\delta_{k,k'}\delta(t - t') \ . \tag{2.44}$$

We will first examine the result of numerical simulations of noise-driven dynamics, and later return to the theoretical analysis.

2.5.1 Noisy Simulations

Previous numerical investigations [11, 13] did not introduce noise in a controlled fashion. We will argue later that some of the phenomena encountered in these simulations can be ascribed to the (uncontrolled) numerical noise. We performed numerical simulations of Eq.(2.5 using a pseudo-spectral method. The time-stepping scheme was chosen as Adams-Bashforth with 2nd order presicion in time. The additive white noise was generated in Fourier-space by choosing η_k for every k from a flat distribution in the interval $[-\sqrt{2\frac{f}{L}}, \sqrt{2\frac{f}{L}}]$. We examined the average steady state velocity of the front as a function of L for fixed f and as a function of f for fixed L. We found the interesting phenomena that are summarized here:

1. In Fig.2.7 we can see two different regimes of the behavior of the average velocity v as a function of the noise $f^{0.5}$ for the fixed system size L. For the noise f smaller then

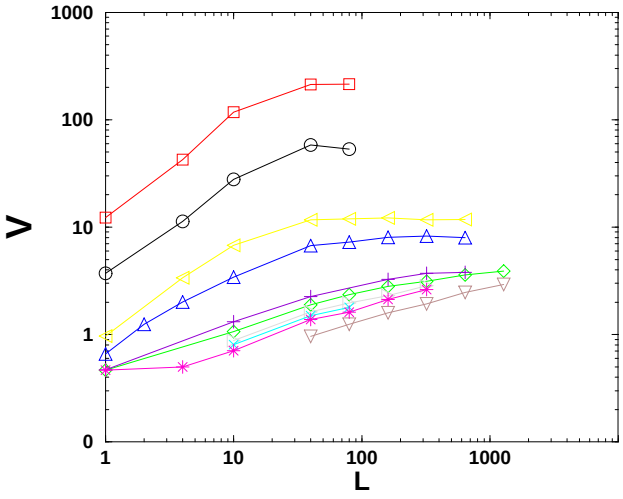

Figure 2.6: The dependence of the average velocity v on the system size L for $f^{0.5} = 0, 2.7 \times 10^{-6}, 2.7 \times 10^{-5}, 2.7 \times 10^{-4}, 2.7 \times 10^{-3}, 2.7 \times 10^{-2}, 2.7 \times 10^{-1}, 0.5, 1.3, 2.7$.

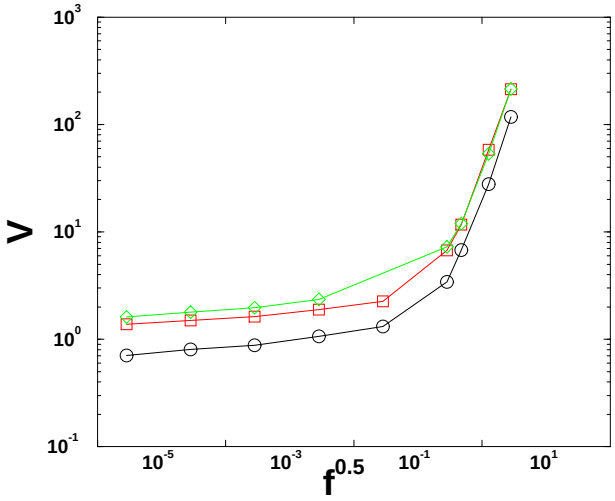

Figure 2.7: The dependence of the average velocity v on the noise $f^{0.5}$ for L=10, 40, 80.

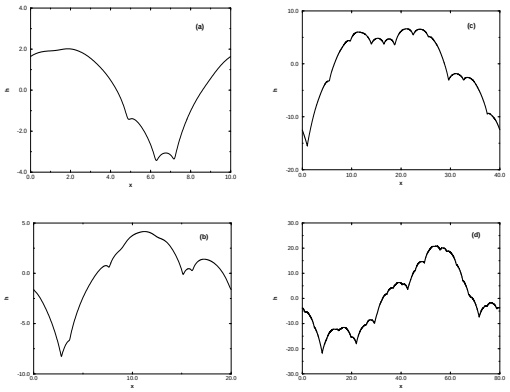

Figure 2.8: Typical flame fronts for $f < f_{cr}$ where the system is sufficientl y small not to be terribly affected by the noise. The effect of noise in this regime is to add additional small cusps to the giant cusp. In figures a-d we present fronts for growing system sizes $\tilde{L} = 10, 20, 40$ and 80 respectively, $\nu = 0.1$. One can observe that when the system size grows there are more cusps with a more complex structure.

same fixed value f_{cr}

$$v \sim f^{\xi} \ . \tag{2.45}$$

For these values of f this dependence is very weak, and $\xi \approx 0.02$. For the large values of f the dependence is much stronger

2. In Fig.2.6 we can see the growth of the average velocity v as a function of the system size L. After some values of L we can see saturation of the velocity. For regime $f < f_{cr}$ the growth of the velocity can be written as

$$v \sim L^{\mu}, \quad \mu \approx 0.35 \pm 0.03 \ . \tag{2.46}$$

3. In Fig.2.8 and Fig.2.9 we can see flame fronts for $f < f_{cr}$ and $f > f_{cr}$.

2.5.2 Calculation of the Number of Poles in the System

The interesting problem that we would like to solve here to better understand the dynamics of poles, is to determine those that exist in our system outside the giant cusp. This can be done by calculating the number of cusps (points of minimum or inflexional points) and their position on the interval $\theta : [0, 2\pi]$ in every moment of time and drawing the positions of the cusps like functions of time, see Fig. 2.10. In this picture we can see the x-positions of all cusps in the system as a function of time.

We have assumed that our system is in a "quasi-stable" state most of the time, i.e. every new cusp that appears in the system includes only one pole. Using pictures obtained in this way we can find:

1. The mean number of poles in the system. By calculating the number of cusps in some moment of time and by investigating the history of every cusp (except the giant cusp), i.e. how many initial cusps take part in formating this cusp, and after averaging the

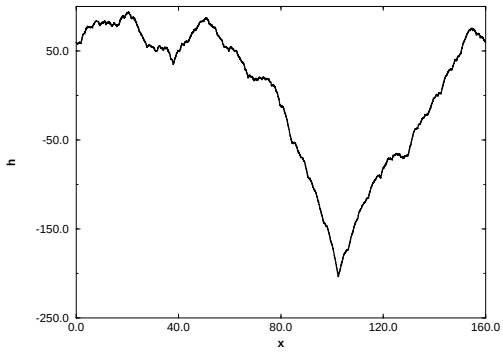

Figure 2.9: A typical flame front for $f > f_{cr}$. The system size is 160. This is sufficient to cause a qualitative change in the appearance of the flame front: the noise introduces significant levels of small scales structure in addition to the cusps.

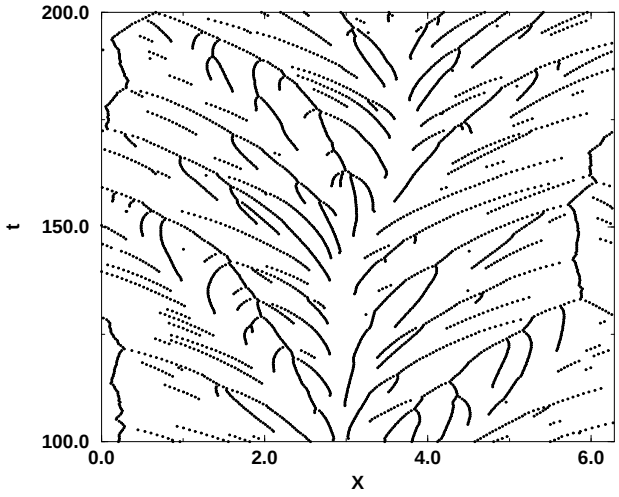

Figure 2.10: The dependence of the cusps positions on timea. $L = 80$ $\nu = 0.1$ $f = 9 \times 10^{-6}$

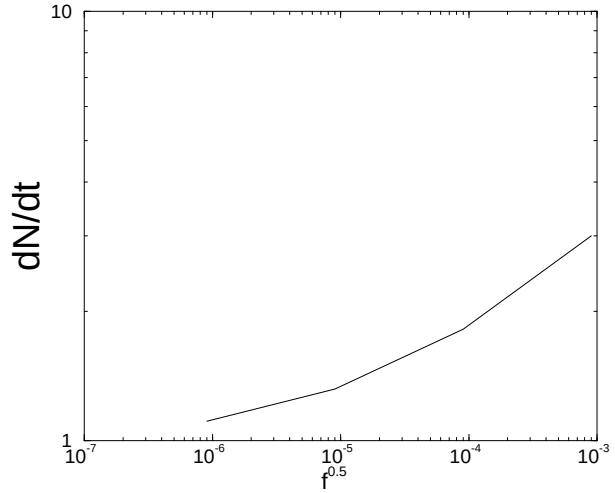

Figure 2.11: The dependence of the pole number in the unit time dN/dt on the noise $f^{0.5}$. $\nu = 0.1$ $L = 80$

number of poles found with respect to different moments of time, we can find the mean number of poles that exist in our system outside the giant cusp. Let us denote this number by δN. There are four regimes that can be defined with respect to the dependence of this number on the noise f:

(i) Regime I: Such little noise that no new cusps exist in our system outside the giant cusp;

(ii) Regime II: Strong dependence of the pole number δN on the noise f;

(iii) Regime III: Saturation of the pole number δN on the noise f, so that this number depends very little on the noise (Fig. 2.12);

$$\delta N \sim f^{0.03} \tag{2.47}$$

The saturated value of δN is defined by next formula (Fig. 2.14, Fig. 2.16)

$$\delta N \approx N(L)/2 \approx \frac{1}{4}\frac{L}{\nu} \tag{2.48}$$

where $N(L) \approx \frac{1}{2}\frac{L}{\nu}$ is the number of poles in the giant cusp.

(iv) Regime IV: We again see a strong dependence of the pole number δN on the noise f (Fig. 2.12);

$$\delta N \sim f^{0.1} \tag{2.49}$$

Because of the numerical noise we can see in most of the simulations only regime III and IV. In the future if no new evidence is seen we will discuss regime III.

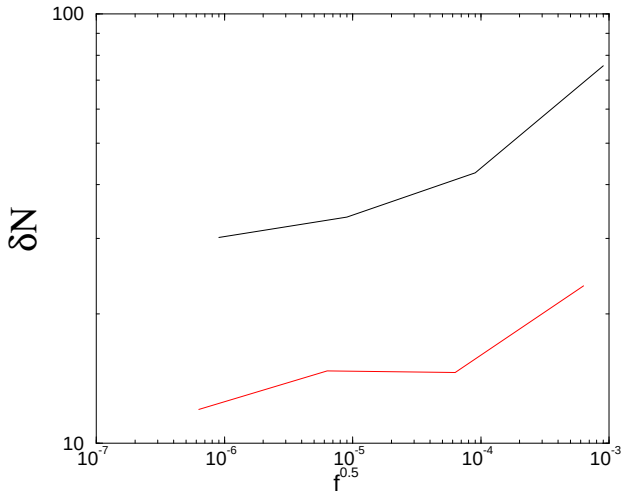

Figure 2.12: The dependence of the excess pole number δN on the noise $f^{0.5}$. $\nu = 0.1$ $L = 40, 80$.

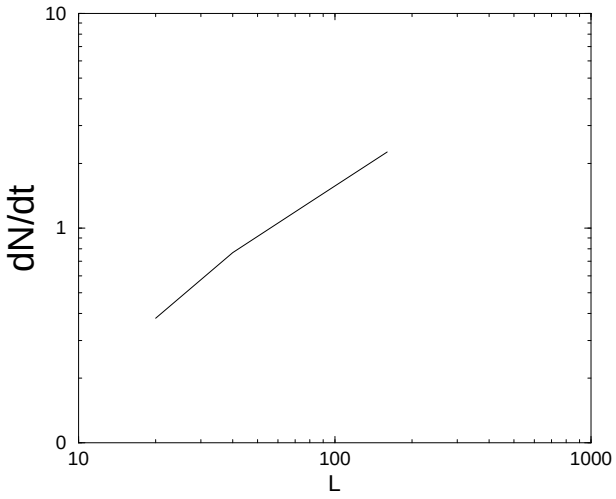

Figure 2.13: The dependence of the pole number in the unit time dN/dt on the system size L. $\nu = 0.1$ $f^{0.5} = 9 \times 10^{-6}$.

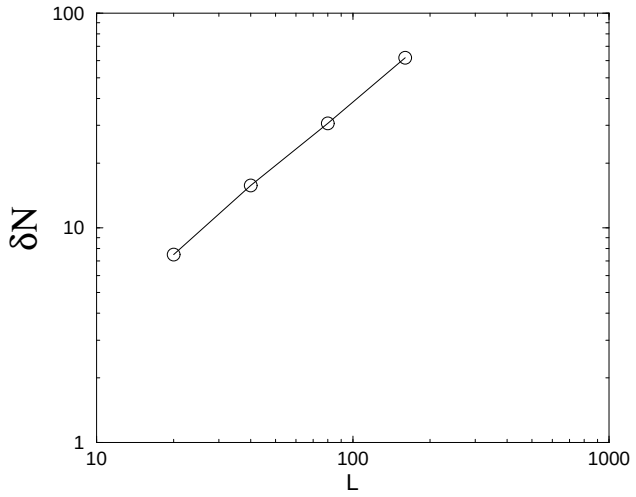

Figure 2.14: The dependence of the excess pole number δN on the system size L. $\nu = 0.1$ $f^{0.5} = 9 \times 10^{-6}$

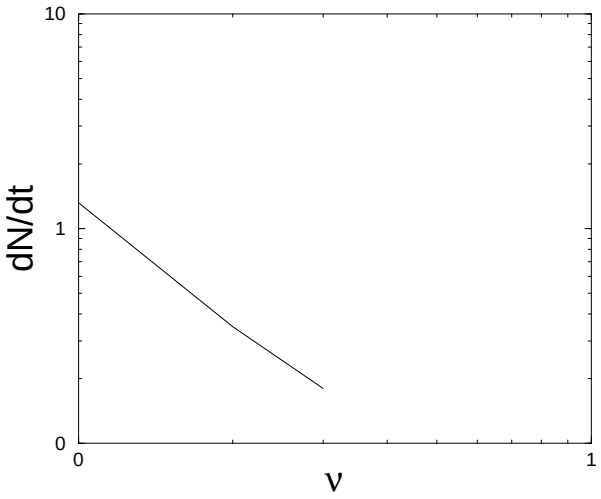

Figure 2.15: The dependence of the pole number in the unit time dN/dt on the parameter ν. $L = 80$ $\nu = 0.1$.

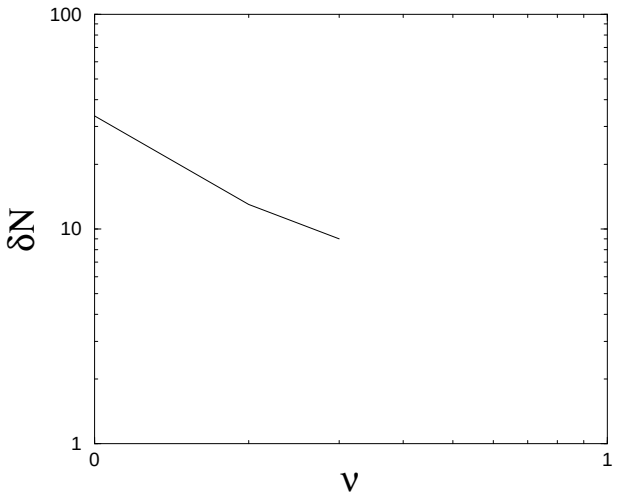

Figure 2.16: The dependence of the excess pole number δN on the the parameter ν. $L = 80$ $\nu = 0.1$.

2. By calculating the new cusp number that appears in the system in the unit time we can find the number of poles that appear in the system in the unit time $\frac{dN}{dt}$. In regime III (Fig. 2.11)

$$\frac{dN}{dt} \sim f^{0.03} \tag{2.50}$$

The dependence on L and ν is defined by (Fig. 2.13 and Fig. 2.15)

$$\frac{dN}{dt} \sim L^{0.8} \tag{2.51}$$

$$\frac{dN}{dt} \sim \frac{1}{\nu^2} \tag{2.52}$$

In regime IV, the dependence on the noise is defined by the following: (Fig. 2.11)

$$\frac{dN}{dt} \sim f^{0.1} \tag{2.53}$$

2.5.3 Theoretical Discussion of the Effect of Noise

The Threshold of Instability to Added Noise. Transition from regime I to regime II

First we present the theoretical arguments that explain the sensitivity of the giant cusp solution to the effect of added noise. This sensitivity increases dramatically with increasing

the system size L. To see this we use again the relationship between the linear stability analysis and the pole dynamics.

Our additive noise introduces perturbations with all k-vectors. We showed previously that the most unstable mode is the $k = 1$ component $A_1 \sin(\theta)$. Thus the most effective noisy perturbation is $\eta_1 \sin(\theta)$ which can potentially lead to a growth of the most unstable mode. Whether or not this mode will grow depends on the amplitude of the noise. To see this clearly we return to the pole description. For small values of the amplitude A_1 we represent $A_1 \sin(\theta)$ as a single pole solution of the functional form $\nu e^{-y} \sin\theta$. The y position is determined from $y = -\log|A_1|/\nu$, and the θ-position is $\theta = \pi$ for positive A_1 and $\theta = 0$ for negative A_1. From the analysis of Section III we know that for very small A_1 the fate of the pole is to be pushed to infinity, independently of its θ position; the dynamics is symmetric in $A_1 \to -A_1$ when y is large enough. On the other hand when the value of A_1 increases the symmetry is broken and the θ position and the sign of A_1 become very important. If $A_1 > 0$ there is a threshold value of y below which the pole is attracted down. On the other hand if $A_1 < 0$, and $\theta = 0$ the repulsion from the poles of the giant cusp grows with decreasing y. We thus understand that qualitatively speaking the dynamics of A_1 is characterized by an asymmetric "potential" according to

$$\dot{A}_1 = -\frac{\partial V(A_1)}{\partial A_1} , \tag{2.54}$$

$$V(A_1) = \lambda A_1^2 - a A_1^3 + \dots . \tag{2.55}$$

¿From the linear stability analysis we know that $\lambda \approx \nu/L^2$, cf. Eq.(1.11). We know further that the threshold for nonlinear instability is at $A_1 \approx \nu^3/L^2$, cf. Eq(2.26). This determines that value of the coefficient $a \approx 2/3\nu^2$. The magnitude of the "potential" at the maximum is

$$V(A_{max}) \approx \nu^7/L^6 . \tag{2.56}$$

The effect of the noise on the development of the mode $A_1 \sin\theta$ can be understood from the following stochastic equation

$$\dot{A}_1 = -\frac{\partial V(A_1)}{\partial A_1} + \eta_1(t) . \tag{2.57}$$

It is well known [41] that for such dynamics the rate of escape R over the "potential" barrier for small noise is proportional to

$$R \sim \frac{\nu}{L^2} \exp^{-\nu^7/fL^5} . \tag{2.58}$$

The conclusion is that any arbitrarily tiny noise becomes effective when the system size increase and when ν decreases. If we drive the system with noise of amplitude $\frac{f}{L}$ the system can always be sensitive to this noise when its size exceeds a critical value L_c that is determined by $f/L_c \sim \nu^7/L_c^6$. This formula defines transition from regime I (no new cusps) to regime II. For $L > L_c$ the noise will introduce new poles into the system. Even numerical noise in simulations involving large size systems may have a macroscopic influence.

The appearance of new poles must increase the velocity of the front. The velocity is proportional to the mean of $(u/L)^2$. New poles distort the giant cusp by additional smaller cusps on the wings of the giant cusp, increasing u^2. Upon increasing the noise amplitude more and more smaller cusps appear in the front, and inevitably the velocity increases. This phenomenon is discussed quantitatively in Section 2.5.

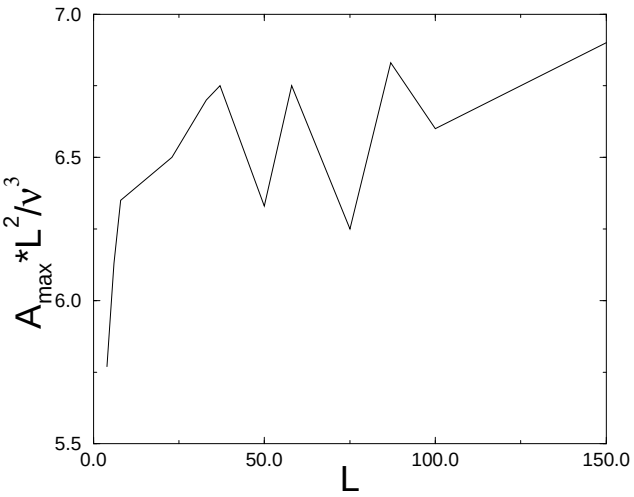

Figure 2.17: The dependence of the normalized amplitude $A_{max}L^2/\nu^3$ on the system size L.

Numerical verifing of the asymmetric "potential" form and dependence of the noise on L_c

From the equations of the motion for poles we can find the distribution of poles in the giant cusp [12]. If we know the distribution of poles in the giant cusp we can then find the form of the "potential" and verify numerically expressions for values λ, A_{max} and $\frac{\partial V(A_1)}{\partial A_1}$ discussed previously. The connection between amplitude A_1 and the position of the pole y is defined by $A_1 = 4\nu e^{-y}$ and the connection between the potential function $\frac{\partial V(A_1)}{\partial A_1}$ and the position of the pole y is defined by formula $\frac{\partial V(A_1)}{\partial A_1} = 4\nu\frac{dy}{dt}e^{-y}$, where $\frac{dy}{dt}$ can be determined from the equation of the motion of the poles. We can find A_{max} as the zero-point of $\frac{\partial V(A_1)}{\partial A_1}$ and λ can be found as $\frac{1}{2}\frac{\partial^2 V(A_1)}{\partial A_1^2}$ for $A_1 = 0$. Numerical measurements were made for the set of values $L = 2n\nu$, where n is a integer and $n > 2$. For our numerical measurements we use the constant $\nu = 0.005$ and the variable L, where L changes in the interval [1,150], or variable ν that changes in the interval [0.005,0.05] and the constant $L = 1$. The results obtained follow:

1. $\frac{A_{max}L^2}{\nu^3}$ as a function of L is almost a constant. (Fig. 2.17)
2. $\frac{A_{max}L^2}{\nu^3}$ as a function of ν is almost a constant. (Fig. 2.18)
3. $\frac{A_{max}}{A_{N(L)}}$ as a function of L is almost a constant. ($A_{N(L)}$ is defined by the position of the upper pole.) (Fig. 2.19)
4. $\frac{A_{max}}{A_{N(L)}}$ as a function of ν is almost a constant. (Fig. 2.20)
5. The value of $\frac{\lambda L^2}{\nu}$ as a function of L is a constant (Fig. 2.21).
6. The value of $\frac{\lambda L^2}{\nu}$ as a function of ν is a constant (Fig. 2.22).

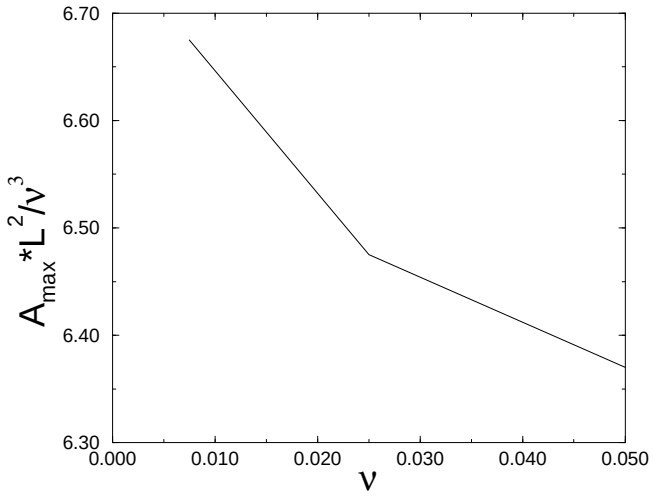

Figure 2.18: The dependence of the normalized amplitude $A_{max}L^2/\nu^3$ on the parameter ν.

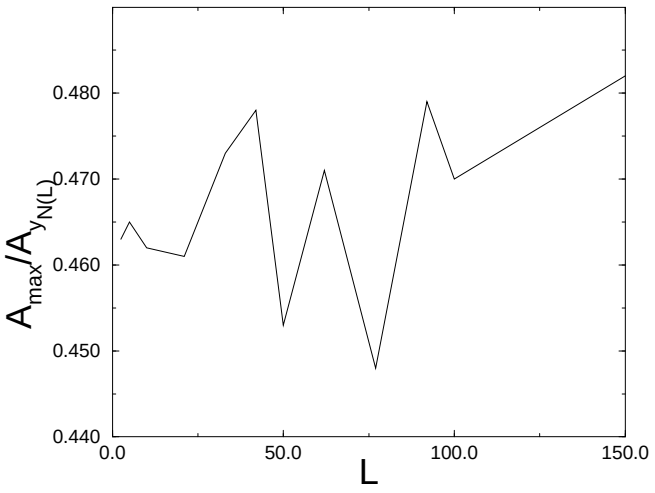

Figure 2.19: The relationship between the amplitude defined by the minimum of the potential A_{max} and the amplitude defined by the position of the upper pole $A_{N(L)}$ as a function of the system size L.

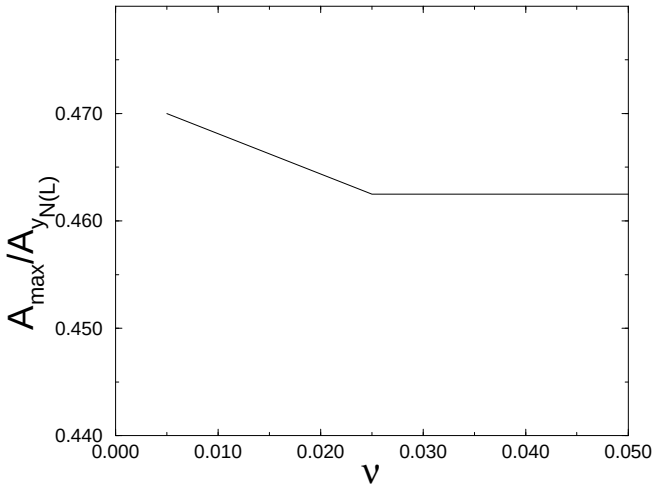

Figure 2.20: The relationship between the amplituda defined by the minimum of the potential A_{max} and the amplitude defined by the position of the upper pole $A_{N(L)}$ as a function of the parameter ν.

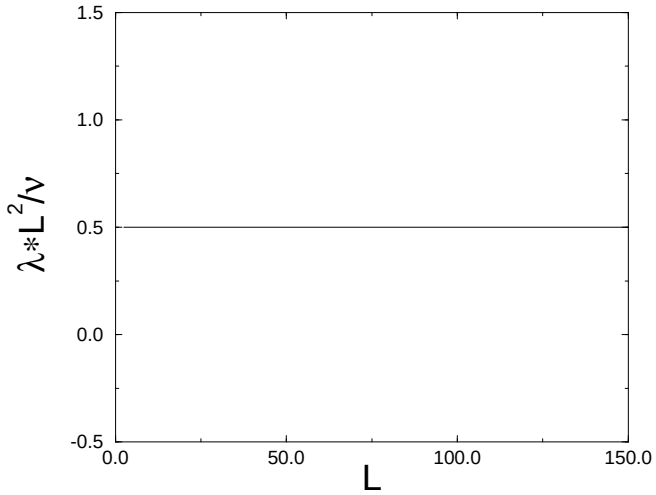

Figure 2.21: The dependence of the normalized parameter $\lambda L^2/\nu$ on the system size L.

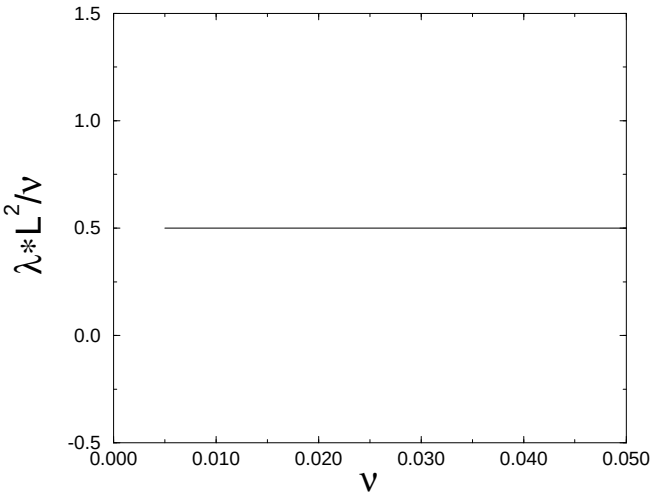

Figure 2.22: The dependence of the normalized parameter $\lambda L^2/\nu$ on the parameter ν.

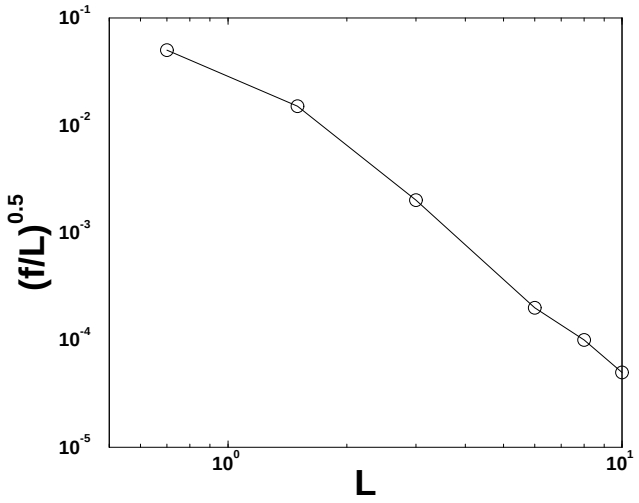

Figure 2.23: The dependence of the critical noise on the system size.

We also verify the boundary between regime I (no new cusps) and regime II (new cusps appear). Fig. 2.23 shows the dependence of $\frac{f}{L_c}$ on L_c. We can see that $f/L_c \sim 1/L_c^6$. These results are in good agreement with the theory.

The Noisy Steady State and its Collapse with Large Noise and System Size

In this subsection we discuss the response of the giant cusp solution to noise levels that are able to introduce a large number of excess poles in addition to those existing in the giant cusp. We will denote the excess number of poles by δN. The first question that we address is how difficult is it to insert yet an additional pole when there is already a given excess δN. To this aim we estimate the effective potential $V_{\delta N}(A_1)$ which is similar to (2.55) but is taking into account the existence of an excess number of poles. A basic approximation that we employ is that the fundamental form of the giant cusp solution is not seriously modified by the existence of an excess number of poles. Of course this approximation breaks down quantitatively already with one excess pole. Qualitatively however it holds well until the excess number of poles is of the order of the original number $N(L)$ of the giant cusp solution. Another approximation is that the rest of the linear modes play no role in this case. At this point we limit the discussion therefore to the situation $\delta N \ll N(L)$ (regime II).

To estimate the parameter λ in the effective potential we consider the dynamics of one pole whose y position y_a is far above y_{max}. According to Eq.(1.11) the dynamics reads

$$\frac{dy_a}{dt} \approx \frac{2\nu(N(L)+\delta N)}{L^2} - \frac{1}{L} \tag{2.59}$$

Since the $N(L)$ term cancels against the L^{-1} term (cf. Sec. II A), we remain with a repulsive term that in the effective potential translates to

$$\lambda = \frac{\nu \delta N}{L^2} \ . \tag{2.60}$$

Next we estimate the value of the potential at the break-even point between attraction and repulsion. In the last subsection we saw that a foreign pole has to be inserted below y_{max} in order to be attracted towards the real axis. Now we need to push the new pole below the position of the existing pole whose index is $N(L) - \delta N$. This position is estimated as in Sec III C by employing the TFH distribution function (2.23). We find

$$y_{\delta N} \approx 2 \ln \Big[\frac{4L}{\pi^2 \nu \delta N} \Big] \ . \tag{2.61}$$

As before, this implies a threshold value of the amplitude of single pole solution $A_{max} \sin\theta$ which is obtained from equating $A_{max} = \nu e^{-y_{\delta N}}$. We thus find in the present case $A_{max} \sim \nu^3 (\delta N)^2 / L^2$. Using again a cubic representation for the effective potential we find $a = 2/(3\nu^2 \delta N)$ and

$$V(A_{max}) = \frac{1}{3} \frac{\nu^7 (\delta N)^5}{L^6} \ . \tag{2.62}$$

Repeating the calculation of the escape rate over the potential barrier we find in the present case

$$R \sim \frac{\nu \delta N}{L^2} \exp^{-\nu^7 (\delta N)^5 / f L^5} \ . \tag{2.63}$$

For a given noise amplitude f there is always a value of L and ν for which the escape rate is of $O(1)$ as long as δN is not too large. When δN increases the escape rate decreases, and eventually no additional poles can creep into the system. The typical number δN for fixed values of the parameters is estimated from equating the argument in the exponent to unity

$$\delta N \approx \left(fL^5/\nu^7\right)^{1/5} \ . \tag{2.64}$$

We can see that δN is strongly dependent on noise f, in contrast to regime III. Let us find the conditions of transition from regime II to III, where we see the saturation of δN with respect to noise f.

(i) We use the expression $A_{max} = 4\nu e^{-y_{\delta N}}$ for the amplitude of the pole solution that equals to $\frac{2\nu \sin\theta}{\cosh(y_{\delta N})-\cos\theta}$; however, this is correct only for the large number $y_{\delta N}$. When $y_{\delta N} < 1$, a better approximation is $A_{max} = \frac{4\nu}{y_{\delta N}^2}$. From the equation (2.61) we find that the boundary value $y_{\delta N} = 1$ corresponds to $\delta N \approx N(L)/2$.

(ii) We use the expression $y_{\delta N} \approx 2\ln\left[\frac{4L}{\pi^2\nu\delta N}\right]$, but for a large value of δN a better approximation that can be found the same way is $y_{\delta N} \approx \frac{\pi^2\nu}{2L}(N(L)-\delta N)\ln\left[\frac{8eL}{\pi^2\nu(N(L)-\delta N)}\right]$ [12]. These expressions give us nearly lthe same result for $\delta N \approx N(L)/2$.

From (i) and (ii) we can make the following conclusions:

(a) The transition from regime II to regime III generally occurs for $\delta N \approx N(L)/2$;

(b) Using the new expressions in (i) and (ii) for the amplitude A_{max} and $y_{\delta N}$, we can determine the noise $\frac{f}{L}$ in regime III by

$$\frac{f}{L} \sim V(A_{max}) \sim \lambda A_{max}^2 \sim \frac{\nu\delta N}{L^2}(\frac{4\nu}{y_{\delta N}^2})^2 \sim \frac{L^2}{\nu}\frac{\delta N}{(N(L)-\delta N)^4} \tag{2.65}$$

This expression defines a very slight dependence of δN on the noise f for $\delta N > N(L)/2$, which explains the noise saturation of δN for regime III.

(c) The form of the giant cusp solution is governed by the poles that are close to zero with respect to y. For the regime III, $N(L)/2$ poles that have positions $y < y_{\delta N=N(L)/2} = 1$ remain at this position. This result explains why the giant cusp solution cannot be seriously modified for regime III.

From eq. (2.64) by using the condition

$$\delta N \approx N(L)/2 \tag{2.66}$$

the boundary noise f_b between regimes II and III can be found as

$$f_b \sim \nu^2 \ . \tag{2.67}$$

The basic equation describing pole dynamics follows

$$\frac{dN}{dt} = \frac{\delta N}{T} \ , \tag{2.68}$$

where $\frac{dN}{dt}$ is the number of poles that appear in the unit time in our system, δN is the excess number of poles, and T is the mean lifetime of a pole (between appearing and merging with the giant cusp). Using the result of numerical simulations for $\frac{dN}{dt}$ and (2.66) we can find for T

$$T = \frac{\delta N}{\frac{dN}{dt}} \sim \nu L^{0.2} \ . \tag{2.69}$$

Thus the lifetime is proportional to ν and depends on the system size L very slightly.

Moreover, the lifetime of a pole is defined by the lifetime of the poles that are in a cusp. From the maximum point of the linear part of Eq.(2.1), we can find the mean character size (Fig.9([28]))

$$\lambda_m \sim \nu \tag{2.70}$$

that defines the size of our cusps. The mean number of poles in a cusp

$$n_{big} \approx \frac{\lambda_m}{2\nu} \sim const \tag{2.71}$$

does not depend on L and ν. The mean number of cusps is

$$N_{big} \sim \frac{\delta N}{n_{big}} \sim \frac{L}{\nu} \ . \tag{2.72}$$

Let us assume that some cusp exists in the main minimum of the system. The lifetime of a pole in such a cusp is defined by three parts.

(I) Time of the cusp formation. This time is proportional to the cusp size (with ln-corrections) and the pole number in the cusp (from pole motion equations)

$$T_1 \sim \lambda_m n_{big} \sim \nu \tag{2.73}$$

(II) Time that the cusp is in the minimum neighborhood. This time is defined by

$$T_2 \sim \frac{a}{v} \tag{2.74}$$

where a is a neighborhood of minimum, such that the force from the giant cusp is smaller than the force from the fluctuations of the excess pole number δN, and v is the velocity of a pole in this neighborhood. Fluctuations of excess pole number δN are expressed as

$$N_{fl} = \sqrt{\delta N} \ . \tag{2.75}$$

From this result and the pole motion equations we find that

$$v \sim \frac{\nu}{L} N_{fl} \sim \frac{\nu}{L}\sqrt{\frac{L}{\nu}} \sim \sqrt{\frac{\nu}{L}} \ . \tag{2.76}$$

The velocity from the giant cusp is defined by

$$v \sim \frac{\nu}{L} N(L) \frac{a}{L} \sim \frac{a}{L} \ . \tag{2.77}$$

So from equating these two equations we obtain

$$a \sim \sqrt{\nu L} \ . \tag{2.78}$$

Thus for T_2 we obtain

$$T_2 \sim \frac{a}{v} \sim L \ . \tag{2.79}$$

(III) Time of attraction to the giant cusp. From the equations of motion for the poles we get

$$T_3 \sim L \ln(\frac{L}{a}) \sim L \ln \sqrt{L} \sim L \ . \tag{2.80}$$

The investigated domain of the system size was found to be

$$T_1 \gg T_2, T_3 \tag{2.81}$$

Therefore full lifetime is

$$T = T_1 + T_2 + T_3 \sim \nu + sL \ , \tag{2.82}$$

where s is a constant and

$$0 < s \ll 1 \ . \tag{2.83}$$

This result qualitatively and partly quantatively explains dependence (2.69). From (2.69), (2.68), (2.66) we can see that in regime III $\frac{dN}{dt}$ is saturated with the system size L.

2.5.4 The acceleration of the flame front because of noise

In this section we estimate the scaling exponents that characterize the velocity of the flame front as a function of the system size. To estimate the velocity of the flame front we need to create an equation for the mean of $< dh/dt >$ given an arbitrary number N of poles in the system. This equation follows directly from (2.4)

$$\left\langle \frac{dh}{dt} \right\rangle = \frac{1}{L^2} \frac{1}{2\pi} \int_0^{2\pi} u^2 d\theta \ . \tag{2.84}$$

After substitution of (2.8) in (2.84) we get, using (2.11) and (2.12)

$$\left\langle \frac{dh}{dt} \right\rangle = 2\nu \sum_{k=1}^{N} \frac{dy_k}{dt} + 2 \left(\frac{\nu N}{L} - \frac{\nu^2 N^2}{L^2} \right) \ . \tag{2.85}$$

Estimating the second and third terms in this equation are straightforward. Writing $N = N(L) + \delta N(L)$ and remembering that $N(L) \sim L/\nu$ and $\delta N(L) \sim N(L)/2$, we find that these terms contribute $O(1)$. The first term contributes only when the current of the poles is asymmetric. Noise introduces poles at a finite value of y_{min}, whereas the rejected poles stream towards infinity and disappear at the boundary of nonlinearity defined by the position of the highest pole as

$$y_{max} \approx 2 \ln \left[\frac{4L}{\pi^2 \nu} \right] \ . \tag{2.86}$$

Thus we have an asymmetry that contributes to the velocity of the front. To estimate the first term let us define

$$d(\sum \frac{dy_k}{dt}) = \sum_{l}^{l+dl} \frac{dy_k}{dt} \ , \tag{2.87}$$

where $\sum_{l}^{l+dl} \frac{dy_k}{dt}$ is the sum over the poles that are on the interval $y : [l, l + dl]$. We can write

$$d(\sum \frac{dy_k}{dt}) = d(\sum \frac{dy_k}{dt})_{up} + d(\sum \frac{dy_k}{dt})_{down} \ , \tag{2.88}$$

where $d(\sum \frac{dy_k}{dt})_{up}$ is the flux of poles moving up and $d(\sum \frac{dy_k}{dt})_{down}$ is the flux of poles moving down.

For these fluxes we can write

$$d(\sum \frac{dy_k}{dt})_{up}, -d(\sum \frac{dy_k}{dt})_{down} \leq \frac{dN}{dt} dl \ . \tag{2.89}$$

So for the first term

$$\begin{aligned} 0 \leq \sum_{k=1}^{N} \frac{dy_k}{dt} &= \int_{y_{min}}^{y_{max}} \frac{d(\sum \frac{dy_k}{dt})}{dl} dl \\ &= \int_{y_{min}}^{y_{max}} \frac{d(\sum \frac{dy_k}{dt})_{up} + d(\sum \frac{dy_k}{dt})_{down}}{dl} dl \\ &\leq \frac{dN}{dt}(y_{max} - y_{min}) \\ &\leq \frac{dN}{dt} y_{max} \end{aligned} \tag{2.90}$$

Because of slight (ln) dependence of y_{max} on L and ν, $\frac{dN}{dt}$ term determines order of nonlinearity for the first term in eq (2.85). This term equals zero for the symmetric current of poles and achieves the maximum for the maximal asymmetric current of poles. A comparison of $v \sim L^{0.42} f^{0.02}$ and $\frac{dN}{dt} \sim L^{0.8} f^{0.03}$ confirms this calculation.

2.6 Summary and Conclusions

The main two messages of this chapter are: (i) There is an important interaction between the instability of developing fronts and random noise; (ii) This interaction and its implications can be understood qualitatively and sometimes quantitatively using the description in terms of complex poles.

The pole description is natural in this context firstly because it provides an exact (and effective) representation of the steady state without noise. Once one succeeds to describe also the *perturbations* about this steady state in terms of poles, one achieves a particularly transparent language for the study of the interplay between noise and instability. This language also allows us to describe in qualitative and semi-quantitative terms the inverse cascade process of increasing typical lengths when the system relaxes to the steady state from small, random initial conditions.

The main conceptual steps in this chapter are as follows: firstly one realizes that the steady state solution, which is characterized by $N(L)$ poles aligned along the imaginary axis is marginally stable against noise in a periodic array of L values. For all values of L the steady state is nonlinearly unstable against noise. The main and foremost effect of noise of a given amplitude f is to introduce an excess number of poles $\delta N(L, f)$ into the system. The existence of this excess number of poles is responsible for the additional wrinkling of the flame front on top of the giant cusp, and for the observed acceleration of the flame front. By considering the noisy appearance of new poles we rationalize the observed scaling laws as a function of the noise amplitude and the system size.

Theoretically we therefore concentrate on estimating $\delta N(L, f)$. We note that some of our consideration are only qualitative. For example, we estimated $\delta N(L, f)$ by assuming that the giant cusp solution is not seriously perturbed. On the other hand we find a flux of poles going to infinity due to the introduction of poles at finite values of y by the noise. The existence of poles spread between y_{max} and infinity *is* a significant perturbation of the giant cusp solution. Thus also the comparison between the various scaling exponents measured and predicted must be done with caution; we cannot guarantee that those cases in which our prediction hit close to the measurement mean that the theory is quantitative. However we believe that our consideration extract the essential ingredients of a correct theory.

The "phase diagram" as a function of L and f in this system consists of three regimes. In the first one, discussed in Section 2.5.3 , the noise is too small to have any effect on the giant cusp solution. In the second the noise introduces excess poles that serve to decorate the giant cusp with side cusps. In this regime we find scaling laws for the velocity as a function of L and f and we are reasonably successful in understanding the scaling exponents. In the third regime the noise is large enough to create small scale structures that are not neatly understood in terms of individual poles. It appears from our numerics that in this regime the roughening of the flame front gains a contribution from the the small scale structure in a way that is reminiscent of *stable*, noise driven growth models like the Kardar-Parisi-Zhang model.

One of our main motivations in this research was to understand the phenomena observed in radial geometry with expanding flame fronts. . We note that many of the insights offered above translate immediately to that problem. Indeed, in radial geometry the flame front accelerates and cusps multiply and form a hierarchic structure as time progresses. Since the radius (and the typical scale) increase in this system all the time, new poles will be added to the system even by a vanishingly small noise. The marginal stability found above holds also in this case, and the system will allow the introduction of excess poles as a result of noise. The results discussed in Ref. [19] can be combined with the present insights to provide a theory of radial growth (chapter 4).

Finally, the success of this approach in the case of flame propagation raises hope that Laplacian growth patterns may be dealt with using similar ideas. A problem of immediate interest is Laplacian growth in channels, in which a finger steady-state solution is known to exist. It is documented that the stability of such a finger solution to noise decreases rapidly with increasing the channel width. In addition, it is understood that noise brings about additional geometric features on top of the finger. There are enough similarities here to indicate that a careful analysis of the analytic theory may shed as much light on that problem as on the present one.

Chapter 3

Using of Pole Dynamics for Stability Analysis of Flame Fronts: Dynamical Systems Approach in the Complex Plane

3.1 Introduction

In this chapter we discuss the stability of steady flame fronts in channel geometry. We write shortly about this topic in chapter 2 (Sec. 2.3) and we want to consider it in detail in this chapter. Traditionally [1–3] one studies stability by considering the linear operator which is obtained by linearizing the equations of motion around the steady solution. The eigenfunctions obtained are *delocalized* and in certain cases are not easy to interpret. In the case of flame fronts the steady state solution is space dependent and therefore the eigenfunctions are very different from simple Fourier modes. We show in this chapter that a good understanding of the nature of the eigenspectrum and eigenmodes can be obtained by doing almost the opposite of traditional stability analysis, i.e., studying the *localized* dynamics of singularities in the complex plane. By reducing the stability analysis to a study of a finite dimensional dynamical system one can gain considerable intuitive understanding of the nature of the stability problem.

The analysis is based on the understanding that for a given channel width L the steady state solution for the flame front is given in terms of $N(L)$ poles that are organized on a line parallel to the imaginary axis [12]. Stability of this solution can then be considered in two steps. In the first step we examine the response of this set of $N(L)$ poles to perturbations in their positions. This procedure yields an important part of the stability spectrum. In the second step we examine general perturbations, which can also be described by the addition of extra poles to the system of $N(L)$ poles. The response to these perturbations gives us the rest of the stability spectrum; the combinations of these two steps rationalizes all the qualitative features found by traditional stability analysis.

In Sec.2 we present the results of traditional linear stability analysis, and show the eigenvalues and eigenfunctions that we want to interpret by using the pole decomposition. Sec. 3 presents the analysis in terms of complex singularities, in two steps as discussed above. A

summary and discussion is presented in Sec.4.

3.2 Linear Stability Analysis in Channel Geometry

The standard technique to study the linear stability of the steady solution is to perturb it by a small perturbation $\phi(\theta,t)$: $u(\theta,t) = u_s(\theta) + \phi(\theta,t)$. Linearizing the dynamics for small ϕ results in the following equation of motion

$$\begin{aligned} \frac{\partial\phi(\theta,t)}{\partial t} &= \frac{1}{L^2}\Big[\partial_\theta[u_s(\theta)\phi(\theta,t)] \\ &+ \nu\partial_\theta^2\phi(\theta,t)\Big] + \frac{1}{L}I(\phi(\theta,t)) \ . \end{aligned} \tag{3.1}$$

were the linear operator contains $u_s(\theta)$ as a coefficient. Accordingly simple Fourier modes do not diagonalize it. Nevertheless, we proceed to decompose $\phi(x)$ in Fourier modes according to ,

$$\phi(\theta,t) = \sum_{k=-\infty}^{\infty} \hat{\phi}_k(t) e^{ik\theta} \tag{3.2}$$

$$u_s(\theta) = -2\nu i \sum_{k=-\infty}^{\infty}\sum_{j=1}^{N} sign(k) e^{-|k|y_j} e^{ik\theta} \tag{3.3}$$

The last equation follows from (2.13) by expanding in a series of $\sin k\theta$. In these sums the discrete k values run over all the integers. Substituting in Eq.(3.1) we get:

$$\frac{d\hat{\phi}_k(t))}{dt} = \sum_n a_{kn}\hat{\phi}_n(t) \ , \tag{3.4}$$

where a_{kn} are entires of an infinite matrix:

$$a_{kk} = \frac{\mid k \mid}{L} - \frac{\nu}{L^2}k^2 \ , \tag{3.5}$$

$$a_{kn} = \frac{k}{L^2} sign(k-n)(2\nu\sum_{j=1}^{N} e^{-|k-n|y_j}) \quad k \neq n \ . \tag{3.6}$$

To solve for the eigenvalues of this matrix we need to truncate it at some cutoff k-vector k^*. The scale k^* can be chosen on the basis of Eq.(3.5) from which we see that the largest value of k for which $a_{kk} \geq 0$ is a scale that we denote as k_{max}, which is the integer part of L/ν. We must choose $k^* > k_{max}$ and test the choice by the convergence of the eigenvalues. The chosen value of k^* in our numerics was $4k_{max}$. One should notice that this cutoff limits the number of eigenvalues, which should be infinite. However the lower eigenvalues will be well represented. The results for the low order eigenvalues of the matrix a_{kn} that were obtained from the converged numerical calculation are presented in Fig.3.1 The eigenvalues are multiplied by L^2/ν and are plotted as a function of L. We order the eigenvalues in decreasing order and denote them as $\lambda_0 \geq \lambda_1 \geq \lambda_2 \ldots$. In addition to the eigenvalues, the truncated matrix also

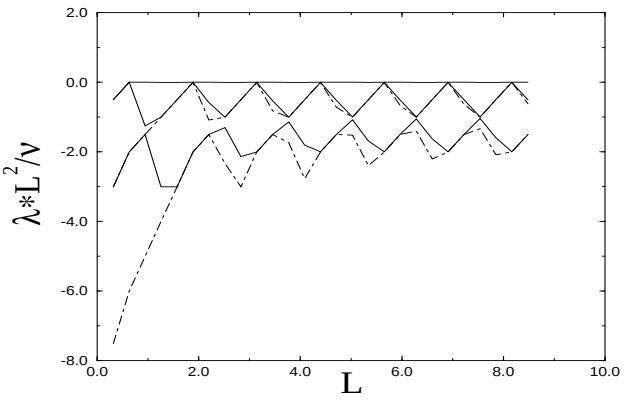

Figure 3.1: A plot of the first five eigenvalues obtained by diagonalizing the matrix obtained by traditional stability analysis, against the system size. The eigenvalues are normalized by L^2/ν. The largest eigenvalue is zero, which is a Goldstone mode. All the other eigenvalues are negative except for the second and third that touch zero periodically. The second and fourth eigenvalues are represented by a solid line and the third and fifth eigenvalues are represented by a dot-dashed line.

yields eigenvectors that we denote as $A^{(\ell)}$. Each such vector has k^* entries, and we can compute the eigenfunctions $f^{(\ell)}(\theta)$ of the linear operator (3.1), using (3.2), as

$$f^{(\ell)}(\theta) \equiv \sum_{-k^*}^{k^*} e^{ik\theta} A_k^{(\ell)} \ . \tag{3.7}$$

Eq.(3.1) does not mix even with odd solutions in θ, as can be checked by inspection. Consequently the available solutions have even or odd parity, expandable in either cos or sin functions. The first two nontrivial eigenfunctions $f^{(1)}(\theta)$ and $f^{(2)}(\theta)$ are shown in Figs.3.2,3.3. a It is evident that the function in Fig.3.2 is odd around zero whereas in Fig.3.3 it is even. Similarly we can numerically generate any other eigenfunction of the linear operator, but we understand neither the physical significance of these eigenfunction nor the L dependence of their associated eigenvalues shown in Fig.3.1 In the next section we will demonstrate how the dynamical system approach in terms of singularities in the complex plane provides us with considerable intuition about these issues.

3.3 Linear Stability in terms of complex singularities

Since the partial differential equation is continuous there is an infinite number of modes. To understand this in terms of pole dynamics we consider the problem in two steps: First, we consider the $2N(L)$ modes associated with the dynamics of the $N(L)$ poles of the giant cusp. In the second step we explain that all the additional modes result from the introduction of additional poles, including the reaction of the $N(L)$ poles of the giant cusp to the new poles. After these two steps we will be able to identify all the linear modes that were found by diagonalizing the stability matrix in the previous section.

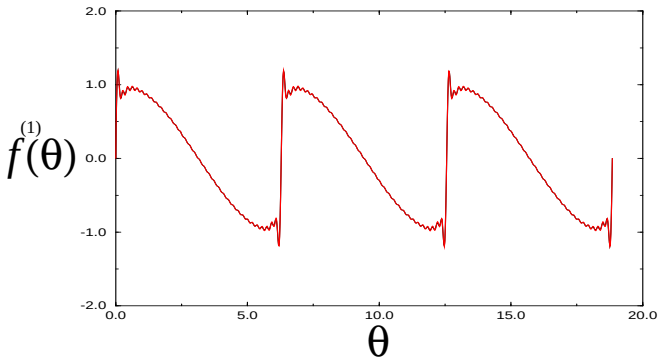

Figure 3.2: The first odd eigenfunction obtained from traditional stability analysis.

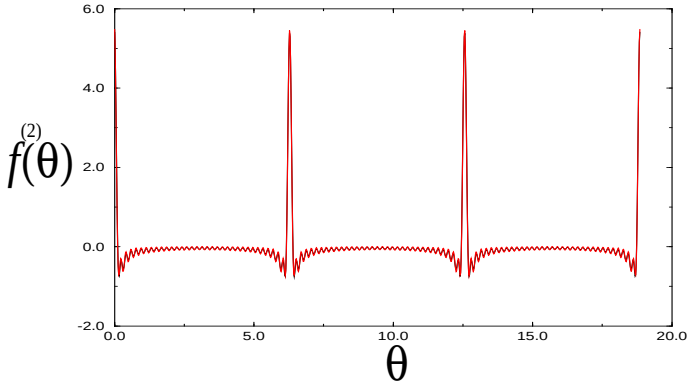

Figure 3.3: The first even eigenfunction obtained from traditional stability analysis.

3.3.1 The modes associated with the giant cusp

In the steady solution all the poles occupy stable equibirilium positions. The forces operating on any given pole cancel exactly, and we can write matrix equations for small perturbations in the pole positions δy_i and δx_i.

Following [12] we rewrite the equations of motion (2.12) using the Lyapunov function U:

$$L\dot{y_i} = \frac{\partial U}{\partial y_i} \tag{3.8}$$

where $i = 1, ..., N$ and

$$\begin{aligned} U = \frac{\nu}{L}[\sum_i \ln\sinh y_i \quad &+ \quad 2\sum_{i<k}(\ln\sinh\frac{y_k - y_i}{2} \\ &+ \quad \ln\sinh\frac{y_k + y_i}{2})] - \sum_i y_i \end{aligned} \tag{3.9}$$

The linearized equations of motion for δy_i are:

$$L\dot{\delta y_i} = \sum_k \frac{\partial^2 U}{\partial y_i \partial y_k}\delta y_k \ . \tag{3.10}$$

The matrix $\partial^2 U/\partial y_i \partial y_k$ is real and symmetric of rank N. We thus expect to find N real eigenvalues and N orthogonal eigenvectors.

For the deviations δx_i in the x positions we find the following linearized equations of motion

$$\begin{aligned} L\dot{\delta x_j} = &-\frac{\nu}{L}\delta x_j \sum_{k=1,k\neq j}^{N}(\frac{1}{\cosh(y_j - y_k) - 1)} \\ &+\frac{1}{\cosh(y_j + y_k) - 1}) \\ &+\frac{\nu}{L}\sum_{k=1,k\neq j}^{N}\delta x_k(\frac{1}{\cosh(y_j - y_k) - 1)} + \frac{1}{\cosh(y_j + y_k) - 1}) \end{aligned} \tag{3.11}$$

In shorthand:

$$L\frac{d\delta x_i}{dt} = V_{ik}\delta x_k \ . \tag{3.12}$$

The matrix V is also real and symmetric. Thus V and $\partial^2 U/\partial y_i \partial y_k$ together supply $2N(L)$ real eigenvalues and $2N(L)$ orthogonal eigenvectors. The explicit form of the matrices V and $\partial^2 U/\partial y_i \partial y_k$ is as follows: For $i \neq k$:

$$\frac{\partial^2 U}{\partial y_i \partial y_k} = \frac{\nu}{L}[\frac{1/2}{\sinh^2(\frac{y_k - y_i}{2})} - \frac{1/2}{\sinh^2(\frac{y_k + y_i}{2})}] \tag{3.13}$$

$$V_{ik} = \frac{\nu}{L}(\frac{1}{\cosh(y_i - y_k) - 1)} + \frac{1}{\cosh(y_i + y_k) - 1}) \tag{3.14}$$

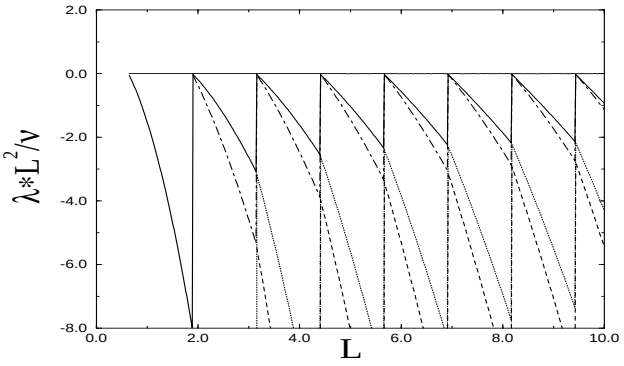

Figure 3.4: The eigenvalues associated with perturbing the positions of the poles that consist the giant cusp. The largest eigenvalue is zero. The second, third, fourth and fifth eigenvalues are represented by a solid line, dot-dashed line, dotted line and dashed line respectively.

and for $i = k$ one gets:

$$\frac{\partial^2 U}{\partial y_i^2} = - \frac{\nu}{L}[\sum_{k\neq i}^{N}\left(\frac{1}{2\sinh^2(\frac{y_k-y_i}{2})}+\frac{1}{2\sinh^2(\frac{y_k+y_i}{2})}\right) + \frac{1}{\sinh^2(y_i)}] \tag{3.15}$$

$$V_{ii} = \sum_{k\neq i}^{N}[-\frac{\nu}{L}(\frac{1}{\cosh(y_i-y_k)-1)}+\frac{1}{\cosh(y_i+y_k)-1})] \tag{3.16}$$

Using the known steady state solutions y_i at any given L we can diagonalize the $N(L)\times N(L)$ matrices numerically. In Fig.3.4 we present the eigenvalues of the lowest order modes obtained from this procedure. The least negative eigenvalues touch zero periodically. This eigenvalue can be fully identified with the motion of the highest pole $y_{N(L)}$ in the giant cusp. At isolated values of L the position of this pole tends to infinity, and then the row and the column in our matrices that contain $y_{N(L)}$ vanish identically, leading to a zero eigenvalue. The rest of the upper eigenvalues match perfectly with half of the observed eigenvalues in Fig.3.1. In other words, the eigenvalues observed here agree perfectly with the ones plotted in this Fig.3.1 until the discontinuous increase from their minimal points. The "second half" of the oscillation in the eigenvalues as a function of L is not contained in this spectrum of the $N(L)$ poles of the giant cusp. To understand the rest of the spectrum we need to consider perturbation of the giant cusp by additional poles. The eigenfunctions can be found using the knowledge of the eigenvectors of these matrices. Let us denote the eigenvectors of $\partial^2 U/\partial y_i \partial y_k$ and V as $a^{(\ell)}$ and $b^{(\ell)}$ respectively. The perturbed solution is explicitly given as (taken for $x_s = 0$):

$$u_s(\theta) + \delta u = 2\nu \sum_{i=1}^{N} \frac{\sin(\theta - \delta x_i)}{\cosh(y_i + \delta y_i) - \cos(\theta - \delta x_i)} \tag{3.17}$$

where δu is

$$\delta u = - 4\nu \sum_{i=1}^{N}\sum_{k=1}^{\infty} \delta y_i k e^{-k y_i} \sin k\theta$$

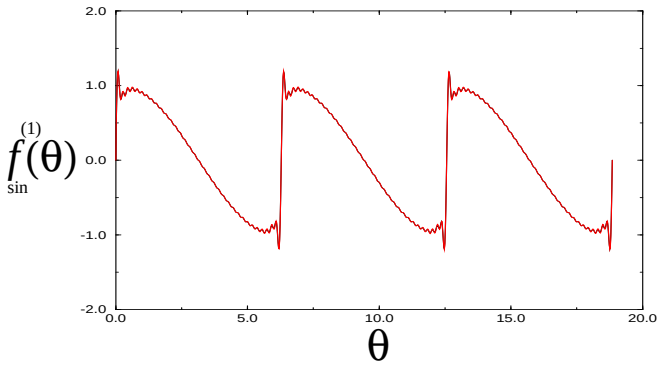

Figure 3.5: The first odd eigenfunction associated with perturbing the positions of the poles in the giant cusp.

$$- \quad 4\nu \sum_{i=1}^{N} \sum_{k=1}^{\infty} \delta x_i k e^{-k y_i} \cos k\theta \tag{3.18}$$

So knowing the eigenvectors $a^{(\ell)}$ and $b^{(\ell)}$ we can estimate the eigenvectors $f^{(\ell)}(\theta)$ of (3.7):

$$f^{(\ell)}_{\sin}(\theta) = -4\nu \sum_{i=1}^{N} \sum_{k=1}^{\infty} a^{(j)}_i k e^{-k y_i} \sin k\theta \ , \quad j = 1, ..., N \tag{3.19}$$

or

$$f^{(\ell)}_{\cos}(\theta) = -4\nu \sum_{i=1}^{N} \sum_{k=1}^{\infty} b^{(j)}_i k e^{-k y_i} \cos k\theta \ , \quad j = 1, ..., N \tag{3.20}$$

where we display separately the sin expansion and the cos expansion. For the case $j = 1$, the eigenvalue is zero, and a uniform translation of the poles in any amount δx_i results in a Goldstone mode. This is characterized by an eigenvector $b^{(1)}_i = 1$ for all i. The eigenvectors $f^{(\ell)}$ (Fig.3.5,3.6)computed this way are identical to numerical precision with those shown in Figs.3.2,3.3, and observe the agreement.

3.3.2 Modes related to additional poles

In this subsection we identify the rest of the modes that were not found in the previous subsection. To this aim we study the response of the TFH solution to the introduction of additional poles. We choose to add M new poles all positioned at the same imaginary coordinate $y_p \ll y_{max}$, distributed at equidistant real positions $\{x_j = x_0 + (2\pi/M)j\}_{j=1}^{M}$. For $x_0 = 0$ we use (2.8) and the Fourier expansion to obtain a perturbation of the form

$$\delta u(\theta, t) \simeq 4\nu M e^{-M y_p(t)} \sin M\theta \tag{3.21}$$

For $x_0 = -\pi/2M$ we get

$$\delta u(\theta, t) \simeq 4\nu M e^{-M y_p(t)} \cos M\theta \tag{3.22}$$

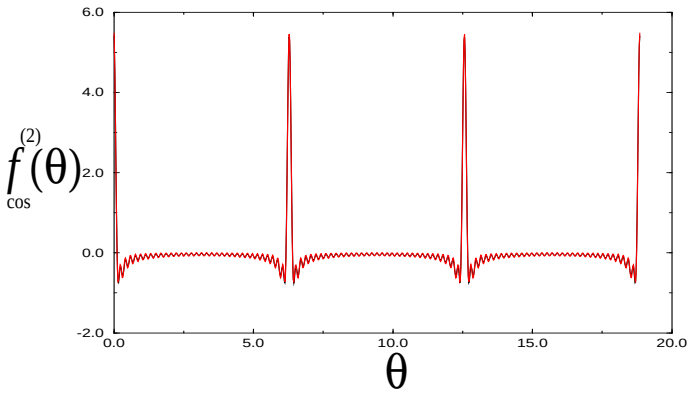

Figure 3.6: The first even eigenfunction associated with perturbing the positions of the poles in the giant cusp.

in both cases the equations for the dynamics of y_p follow from Eqs.(2.11)-(2.12):

$$\frac{dy_p}{dt} \simeq 2\frac{\nu}{L^2}\alpha(M) \ , \tag{3.23}$$

where $\alpha(M)$ is given as:

$$\alpha(M) = [\frac{1}{2}(\frac{L}{\nu}+1)] - \frac{1}{2}(\frac{L}{\nu} - M) \tag{3.24}$$

Since (3.23) is linear, we can solve it and substitute in Eqs.(3.21)-(3.22). Seeking a form $\delta u(\theta,t) \sim exp(-\lambda(M)t)$ we find that the eigenvalue $\lambda(M)$ is

$$\lambda(M) = 2M\frac{\nu}{L^2}\alpha(M) \tag{3.25}$$

These eigenvalues are plotted in Fig.3.7 At this point we consider the dynamics of the poles in the giant cusp under the influence of the additional M poles. From Eqs.(3.10), (3.12), (2.11), (2.12) we obtain, after some obvious algebra,

$$L\dot{\delta y_i} = \sum_j \frac{\partial^2 U}{\partial y_i \partial y_j}\delta y_j - 4\frac{\nu}{L}Me^{-My_p(t)}\sinh(My_i) \tag{3.26}$$

or

$$L\dot{\delta x_i} = \sum_j V_{ij}\delta x_j - 4\frac{\nu}{L}Me^{-My_p(t)}\cosh(My_i) \tag{3.27}$$

It is convenient now to transform from the basis δy_i to the natural basis w_i which is obtained using the linear transformation $w = A^{-1}\delta y$. Here the matrix A has columns which are the eigenvectors of $\partial^2 U/\partial y_i \partial y_j$ which were computed before. Since the matrix was real symmetric, the matrix A is orthogonal, and $A^{-1} = A^T$. Define $C = 4\frac{\nu}{L^2}Me^{-My_p(0)}$ and write

$$\dot{w_i} = -\lambda_i w_i - Ce^{-\lambda(M)t}\xi_i \ , \tag{3.28}$$

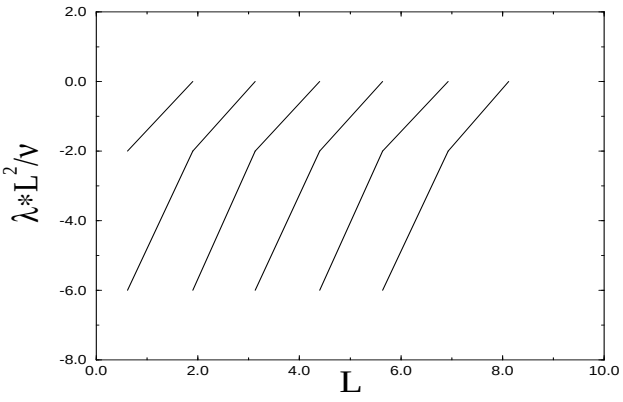

Figure 3.7: Spectrum of eigenvalues associated with the reaction of the poles in the giant cusp to the addition of new poles.

where $-\lambda_i$ are the eigenvalues associated with the columns of A, and

$$\xi_i = \sum_j A_{ji} \sinh M y_j \ . \tag{3.29}$$

We are looking now for a solution that decays exponentially at the rate $\lambda(M)$:

$$w_i(t) = w_i(0) e^{-\lambda(M) t} \tag{3.30}$$

Substituting the desired solution in (3.28) we find a condition on the initial value of w_i:

$$w_i(0) = -\frac{C}{\lambda_i - \lambda(M)} \xi_i \tag{3.31}$$

Transforming back to δy_i we get

$$\begin{aligned} \delta y_i(0) &= \sum_k A_{ik} w_k(0) = -\sum_k A_{ik} \frac{C}{\lambda_k - \lambda(M)} \sum_l A_{lk} \sinh M y_l \\ &= -C \sum_l \sinh M y_l \sum_k \frac{A_{ik} A_{lk}}{\lambda_k - \lambda_p^M} \end{aligned} \tag{3.32}$$

We can get the eigenfunctions of the linear operator, as before, using Eqs.(3.18), (3.21), (3.22), (3.32). We get

$$\begin{aligned} f_{\sin}^{(M)}(\theta) &= 4C\nu \sum_{i=1}^{N(L)} \sum_{k=1}^{\infty} (\sum_l \sinh M y_l \sum_m \frac{A_{im} A_{lm}}{\lambda_m - \lambda(M)}) \\ &\times k e^{-k y_i} \sin k\theta + L^2 C \sin M\theta \end{aligned} \tag{3.33}$$

An identical calculation to the one started with Eq. (3.28) can be followed for the deviations δx_i. The final result reads

$$\begin{aligned} f_{\cos}^{(M)}(\theta) &= 4C\nu \sum_{i=1}^{N(L)} \sum_{k=1}^{\infty} (\sum_l \cosh M y_l \sum_m \frac{\tilde{A}_{im} \tilde{A}_{lm}}{\tilde{\lambda}_m - \lambda(M)}) \\ &\times k e^{-k y_i} \cos k\theta + L^2 C \cos M\theta \ , \end{aligned} \tag{3.34}$$

where $\tilde{A}$ is the matrix whose columns are the eigenvectors of V, and $-\tilde{\lambda}_i$ its eigenvalues.

We are now in position to explain the entire linear spectrum using the knowledge that we have gained. The spectrum consists of two separate types of contributions. The first type has $2N$ modes that belong to the dynamics of the unperturbed $N(L)$ poles in the giant cusp. The second part, which is most of the spectrum, is built from modes of the second type since M can go to infinity. This structure is seen in the Fig.3.4 and Fig.3.7.

We can argue that the set of eigenfunctions obtained above is complete and exhaustive. To do this we show that any arbitrary periodic function of θ can be expanded in terms of these eigenfunctions. Start with the standard Fourier series in terms of sin and cos functions. At this point solve for $\sin k\theta$ and $\cos k\theta$ from Eqs.(3.33-3.34). Substitute the results in the Fourier sums. We now have an expansion in terms of the eigenmodes $f^{(M)}$ and in terms of the triple sums. The triple sums however can be expanded, using Eqs.(3.19-3.20), in terms of the eigenfunctions $f^{(\ell)}$. We can thus decompose any function in terms of the eigenfunctions $f^{(M)}$ and $f^{(\ell)}$.

3.4 Conclusions

We discussed the stability of flame fronts in channel geometry using the representation of the solutions in terms of singularities in the complex plane. In this language the stationary solution, which is a giant cusp in configuration space, is represented by $N(L)$ poles which are organized on a line parallel to the imaginary axis. We showed that the stability problem can be understood in terms of two types of perturbations. The first type is a perturbation in the positions of the poles that make up the giant cusp. The longitudinal motions of the poles give rise to odd modes, whereas the transverse motions to even modes. The eigenvalues associated with these modes are eigenvalues of a finite, real and symmetric matrices, cf. Eqs.(3.13), (3.14), (3.15), (3.16). The second type of perturbations is obtained by adding poles to the set of $N(L)$ poles representing the giant cusp. The reaction of the latter poles is again separated into odd and even functions as can be seen from Eqs.(3.21), (3.22). Together the two types of perturbations rationalize and explain all the features of the eigenvalues and eigenfunctions obtained from the standard linear stability analysis.

Chapter 4

Dynamics and Wrinkling of Radially Propagating Fronts Inferred from Scaling Laws in Channel Geometries

4.1 Introduction

The main idea of this chapter is that in order to derive scaling laws for unstable front propagation in radial geometry, it is useful to study noisy propagation in channel geometries, in which the noiseless dynamics results usually in simple shapes of the advancing fronts [1].

The understanding of radial geometries requires control of the effect of noise on the unstable dynamics of propagation. It is particularly difficult to achieve such a control in radial geometries due to the vagueness of the distinction between external noise and noisy initial conditions. Channel geometries are simpler when they exhibit a stable solution for growth in the noiseless limit. One can then study the effects of external noise in such geometries without any ambiguity. If one finds rules to translate the resulting understanding of the effects of noise in channel growth to radial geometries, one can derive the scaling laws in the later situation in a satisfactory manner. We will exemplify the details of such a translation in the context of premixed flames that exist as self sustaining fronts of exothermic chemical reactions in gaseous combustion. But our contention is that similar ideas should be fruitful also in other contexts of unstable front propagation. Needless to say, there are aspects of the front dynamics and statistics in the radial geometry that *cannot* be explained from observations of fronts in a channel geometry; examples of such aspects are discussed at the end of this chapter.

Mathematically our example is described [11] by an equation of motion for the angle-dependent modulus of the radius vector of the flame front, $R(\theta, t)$:

$$\begin{aligned} \frac{\partial R}{\partial t} &= \frac{U_b}{2{R_0}^2(t)}\left(\frac{\partial R}{\partial \theta}\right)^2 + \frac{D_M}{{R_0}^2(t)}\frac{\partial^2 R}{\partial \theta^2} \\ &+ \frac{\gamma U_b}{2R_0(t)} I(R) + U_b \ . \end{aligned} \tag{4.1}$$

Here $0< \theta < 2\pi$ is an angle and the constants U_b, D_M and γ are the front velocity for an ideal cylindrical front, the Markstein diffusivity and the thermal expansion coefficient respectively.

$R_0(t)$ is the mean radius of the propagating flame:

$$R_0(t) = \frac{1}{2\pi}\int_0^{2\pi} R(\theta,t)d\theta \ . \tag{4.2}$$

The functional $I(R)$ is best represented in terms of its Fourier decomposition. Its Fourier component is $|k|R_k$ where R_k is the Fourier component of R. Simulations of this equation, as well as experiments in the parameter regime for which this equation is purportedly relevant, indicate that for large times R_0 grows as a power in time

$$R_0(t) = (const + t)^{\beta} \ , \tag{4.3}$$

with $\beta > 1$, and that the width of the interface W grows with R_0 as

$$W(t) \sim R_0(t)^{\chi} \ , \tag{4.4}$$

with $\chi < 1$.

4.2 The Geometry of Developing Flame Fronts: Analysis with Pole Decomposition

The study of growing fronts in nonlinear physics [1] offers fascinating examples of spontaneous generation of fractal geometry [2, 3]. Advancing fronts rarely remain flat; usually they form either fractal objects with contorted and ramified appearance, like Laplacian growth patterns and diffusion limited agregates (DLA) [31], or they remain graphs, but they "roughen" in the sense of producing self-affine fractals whose "width" diverges with the linear scale of the system with some characteristic exponent. The study of interface growth where the roughening is caused by the noisy environment, with either annealed or quenched noise, was a subject of active research in recent years [32, 33]. These studies met considerable success and there is significant analytic understanding of the nature of the universality classes that can be expected. The study of interface roughening in system in which the flat surface is inherently unstable is less developed. One interesting example that attracted attention is the Kuramoto-Sivashinsky equation [9, 34] which is known to roughen in 1+1 dimensions but is claimed not to roughen in higher dimensions [42]. Another outstanding example is Laplacian growth patterns [35]. This chapter is motivated by a new example of the dynamics of outward propagating flames whose front wrinkles and fractalizes [11]. We will see that this problem has many features that closely resemble Laplacian growth, including the existence of a single finger in channel growth versus tip splitting in cylindrical outward growth, extreme sensitivity to noise, etc. In the case of flame fronts the equation of motion is amenable to analytic solutions and as a result we can understand some of these issues.

The physical problem that motivates this analysis is that of pre-mixed flames which exist as self-sustaining fronts of exothermic chemical reactions in gaseous combustion. It had been known for some time that such flames are intrinsically unstable [43]. It was reported that such flames develop characteristic structures which includes cusps, and that under usual experimental conditions the flame front accelerates as time goes on [10]. In recent work Filyand et al. [11] proposed an equation of motion that is motivated by the physics and

seems to capture a number of the essential features of the observations. The equation is written in cylindrical geometry and is for $R(\theta,t)$ which is the modulus of the radius vector on the flame front:

$$\begin{aligned}\frac{\partial R}{\partial t} &= \frac{U_b}{2{R_0}^2(t)}\left(\frac{\partial R}{\partial \theta}\right)^2 + \frac{D_M}{{R_0}^2(t)}\frac{\partial^2 R}{\partial \theta^2} \\ &+ \frac{\gamma U_b}{2R_0(t)} I(R) + U_b \ .\end{aligned} \tag{4.5}$$

Here $0< \theta < 2\pi$ is an angle and the constants U_b, D_M and γ are the front velocity for an ideal cylindrical front, the Markstein diffusivity and the thermal expansion coefficient respectively. $R_0(t)$ is the mean radius of the propagating flame:

$$R_0(t) = \frac{1}{2\pi}\int_0^{2\pi} R(\theta,t)d\theta \ . \tag{4.6}$$

The functional $I(R)$ is best represented in terms of its Fourier decomposition. Its Fourier component is $|k|R_k$ where R_k is the Fourier component of R.

Numerical simulations of the type reported in ref. [11] are presented in Fig.4.1. The two most prominent features of these simulations are the wrinkled multi-cusp appearance of the fronts and its acceleration as time progresses. One observes the phenomenon of tip splitting in which new cusps are added to the growing fronts between existing cusps. Both experiments and simulations indicate that for large times R_0 grows as a power in time

$$R_0(t) = (const + t)^{\beta} \ , \tag{4.7}$$

with $\beta > 1$, (of the order of 1.5) and that the width of the interface W grows with R_0 as

$$W(t) \sim R_0(t)^{\chi} \ , \tag{4.8}$$

with $\chi < 1$ (of the order of 2/3). The understanding of these two features and the derivation of the scaling relation between β and χ are the main aims of this chapter.

Equation (4.6) can be written as a one-parameter equation by rescaling R and t according to $r \equiv RU_b/D_M$, $\tau \equiv tU_b^2/D_M$. Computing the derivative of Eq.(4.6) with respect to θ and substituting the dimensionless variables one obtains:

$$\frac{\partial u}{\partial \tau} = \frac{u}{r_0^2}\frac{\partial u}{\partial \theta} + \frac{1}{r_0^2}\frac{\partial^2 u}{\partial \theta^2} + \frac{\gamma}{2r_0} I\{u\} \ . \tag{4.9}$$

where $u \equiv \frac{\partial r}{\partial \theta}$. To complete this equation we need a second one for $r_0(t)$, which is obtained by averaging (4.6) over the angles and rescaling as above. The result is

$$\frac{dr_0}{d\tau} = \frac{1}{2r_0^2}\frac{1}{2\pi}\int_0^{2\pi} u^2 d\theta + 1 \ . \tag{4.10}$$

These two equations are the basis for further analysis

Following [12, 14–16, 38, 39] we expand now the solutions $u(\theta,\tau)$ in poles whose position $z_j(\tau) \equiv x_j(\tau) + iy_j(\tau)$ in the complex plane is time dependent:

$$\begin{aligned} u(\theta,\tau) &= \sum_{j=1}^{N} \cot\left[\frac{\theta - z_j(\tau)}{2}\right] + c.c. \\ &= \sum_{j=1}^{N} \frac{2\sin[\theta - x_j(\tau)]}{\cosh[y_j(\tau)] - \cos[\theta - x_j(\tau)]} \ , \end{aligned} \tag{4.11}$$

$$r(\theta,\tau) = 2\sum_{j=1}^{N} \ln\Big[\cosh(y_j(\tau)) - \cos(\theta - x_j(\tau))\Big] + C(\tau) \ . \tag{4.12}$$

In (4.12) $C(\tau)$ is a function of time. The function (4.12) is a superposition of quasi-cusps (i.e. cusps that are rounded at the tip). The real part of the pole position (i.e. x_j) describes the angle coordinate of the maximum of the quasi-cusp, and the imaginary part of the pole position (i.e y_j) is related the height of the quasi-cusp. As y_j decreases (increases) the height of the cusp increases (decreases). The physical motivation for this representation of the solutions should be evident from Fig.4.1.

The main advantage of this representation is that the propagation and wrinkling of the front can be described now via the dynamics of the poles and of $r_0(t)$. Substituting (4.11) in (4.9) we derive the following ordinary differential equations for the positions of the poles:

$$-r_0^2 \frac{dz_j}{d\tau} = \sum_{k=1,k\neq j}^{2N} \cot\left(\frac{z_j - z_k}{2}\right) + i\frac{\gamma r_0}{2} sign[Im(z_j)] \ . \tag{4.13}$$

After substitution of (4.11) in (4.10) we get, using (4.13) the ordinary differential equation for r_0,

$$\frac{dr_0}{d\tau} = 2\sum_{k=1}^{N} \frac{dy_k}{d\tau} + 2\left(\frac{\gamma}{2}\frac{N}{r_0} - \frac{N^2}{r_0^2}\right) + 1 \ . \tag{4.14}$$

In our problem the outward growth introduces important modifications to the channel results. The number of poles in a stable configuration is proportional here to the radius r_0 instead of L, but the former grows in time. The system becomes therefore unstable to the addition of new poles. If there is noise in the system that can generate new poles, they will not be pushed toward infinite y. It is important to stress that any infinitesimal noise (either numerical or experimental) is sufficient to generate new poles. These new poles do not necessarily merge their x-positions with existing cusps. Even though there is attraction along the real axis as in the channel case, there is a stretching of the distance between the poles due to the radial growth. This may counterbalance the attraction. Our first new idea is that these two opposing tendencies define a typical scale denoted as $\mathcal{L}$. if we have a cusp that is made from the x-merging of N_c poles on the line $x = x_c$ and we want to know whether a x-nearby pole with real coordinate x_1 will merge with this large cusp, the answer depends on the distance $D = r_0|x_c - x_1|$. There is a length $\mathcal{L}(N_c, r_0)$ such that if $D > \mathcal{L}(N_c, r_0)$ then the single cusp will never merge with the larger cusp. In the opposite limit the single cusp will move towards the large cusp until their x- position merges and the large cusp will have $N_c + 1$ poles.

This finding stems directly from the equations of motion of the N_c x-merged poles and the single pole at x_1. First note that from Eq.4.7 (which is not explained yet) it follows that asymptotically $r_0(\tau) = (a+\tau)^\beta$ where $r_0(0) = a^\beta$. Next start from 4.13 and write equations for the angular distance $x = x_1 - x_c$. It follows that for any configuration y_j along the imaginary axis

$$\frac{dx}{d\tau} \leq -\frac{2N_c \sin x[1-\cos x]^{-1}}{(a+\tau)^{2\beta}} = -\frac{2N_c \cot(\frac{x}{2})}{(a+\tau)^{2\beta}} \ . \tag{4.15}$$

For small x we get

$$\frac{dx}{d\tau} \leq -\frac{4N_c}{x(a+\tau)^{2\beta}} \ . \tag{4.16}$$

The solution of this equation is

$$x(0)^2 - x(\tau)^2 \geq \frac{8N_c}{2\beta-1}(a^{1-2\beta} - (a+\tau)^{1-2\beta}) \ . \tag{4.17}$$

To find $\mathcal{L}$ we set $x(\infty) > 0$ from which we find that the angular distance will remain finite as long as

$$x(0)^2 > \frac{8N_c}{2\beta-1}a^{1-2\beta} \ . \tag{4.18}$$

Since $r_0 \sim a^\beta$ we find the threshold angle x^*

$$x^* \sim \sqrt{N}_c r_0^{\frac{(1-2\beta)}{2\beta}} \ , \tag{4.19}$$

above which there is no merging between the giant cusp and the isolated pole. To find the actual distance $\mathcal{L}(N_c, r_0)$ we multiply the angular distance by r_0 and find

$$\mathcal{L}(N_c, r_0) \equiv r_0 x^* \sim \sqrt{N_c} r_0^{\frac{1}{2\beta}} \ . \tag{4.20}$$

To understand the geometric meaning of this result we recall the features of the TFH cusp solution. Having a typical length L the number of poles in the cusp is linear in L. Similarly, if we have in this problem two cusps a distance $2\mathcal{L}$ apart, the number N_c in each of them will be of the order of $\mathcal{L}$. From (4.20) it follows that

$$\mathcal{L} \sim r_0^{\frac{1}{\beta}} \ . \tag{4.21}$$

For $\beta > 1$ the circumference grows faster than $\mathcal{L}$, and therefore at some points in time poles that appear between two large cusps would not be attracted toward either, and new cusps will appear. We will show later that the most unstable positions to the appearance of new cusps are precisely the midpoints between existing cusps. This is the mechanism for the addition of cusps in analogy with tip splitting in Laplacian growth.

We can now estimate the width of the flame front as the height of the largest cusps. Since this height is proportional to $\mathcal{L}$ (cf. property (v) of the TFH solution), Eq.(4.21) and Eq.(4.8) lead to the scaling relation

$$\chi = 1/\beta \ . \tag{4.22}$$

This scaling law is expected to hold all the way to $\beta = 1$ for which the flame front does not accelerate and the size of the cusps becomes proportional to r_0.

In channels there is a natural lengthscale, the width $\tilde{L}$ of the channel. The translation of channel results to radial geometry will be based on the identification in the latter context of the time dependent scale $\mathcal{L}(t)$ that plays the role of $\tilde{L}$ in the former. To do this we need first to review briefly the main pertinent results for noisy channel growth. In channel geometry the equation of motion is written in terms of the position $h(x,t)$ of the flame front above the x-axis. After appropriate rescalings [12] it reads:

$$\frac{\partial h(x,t)}{\partial t} = \frac{1}{2}\left[\frac{\partial h(x,t)}{\partial x}\right]^2 + \nu\frac{\partial^2 h(x,t)}{\partial x^2} + I\{h(x,t)\} + 1. \tag{4.23}$$

It is convenient to rescale the domain size further to $0 < \theta < 2\pi$, and to change variables to $u(\theta,t) \equiv \partial h(\theta,t)/\partial\theta$. In terms of this function we find

$$\frac{\partial u(\theta,t)}{\partial t} = \frac{u(\theta,t)}{L^2}\frac{\partial u(\theta,t)}{\partial \theta} + \frac{\nu}{L^2}\frac{\partial^2 u(\theta,t)}{\partial \theta^2} + \frac{1}{L} I\{u(\theta,t)\} \tag{4.24}$$

where $L = \tilde{L}/2\pi$. In noiseless conditions this equation admits exact solutions that are represented in terms of N poles whose position $z_j(t) \equiv x_j(t) + iy_j(t)$ in the complex plane is time dependent:

$$u(\theta,t) = \nu \sum_{j=1}^{N} \cot\left[\frac{\theta - z_j(t)}{2}\right] + c.c.\ , \tag{4.25}$$

The steady state for channel propagation is unique and linearly stable; it consists of $N(L)$ poles which are aligned on one line parallel to the imaginary axis. The geometric appearance of the flame front is a giant cusp, analogous to the single finger in the case of Laplacian growth in a channel. The height of the cusp is proportional to L, and the propagation velocity is a constant of the motion. The number of poles in the giant cusp is linear in L Eq. (1.10,

The introduction of additive random noise to the dynamics changes the picture qualitatively. It is convenient to add noise to the equation of motion in Fourier representation by adding a white noise η_k for every k mode. The noise correlation function satisfies the relation $< \eta_k(t)\eta_{k'}(t') >= \delta_{k,k'}\delta(t-t')f/L$. The noise in our simulations is taken from a flat distribution in the interval $[-\sqrt{2f/L}, \sqrt{2f/L}]$; this guarantees that when the system size changes, the typical noise per unit length of the flame front remains constant. It was shown in chapter 2 and [17] that for moderate but fixed noise levels the average velocity v of the front increases with L as a power law. In our present simulations we found

$$v \sim L^{\mu}\ , \quad \mu \approx 0.35 \pm 0.03\ . \tag{4.26}$$

For a fixed system size L the velocity has also a power law dependence on the level of the noise, but with a much smaller exponent: $v \sim f^{\xi}\ , \quad \xi \approx 0.02$. These results were understood theoretically by analysing the noisy creation of new poles that interact with the poles defining the giant cusp (in chapter 2 and [17]).

Next we shed light on phenomenon of tip splitting that here is seen as the addition of new cusps roughly in between existing ones. We mentioned the instability toward the addition of new poles. We argue now that the tip between the cusps is most sensitive to pole creation. This can be shown in both channel and radial geometry. For example consider a TFH-giant cusp solution in which all the poles are aligned (without loss of generality) on the $x = 0$ line.

Add a new pole in the complex position (x_a, y_a) to the existing $N(L)$ poles, and study its fate. It can be shown that in the limit $y_a \to \infty$ (which is the limit of a vanishing perturbation of the solution) the equation of motion is

$$\frac{dy_a}{dt} = \frac{2\pi\nu}{L^2}(2N(L)+1) - 1 \qquad y_a \to \infty \ . \tag{4.27}$$

Since $N(L)$ satisfies (1.10) this equation can be rewritten as

$$\frac{dy_a}{dt} = \frac{4\pi\nu}{L^2}(1-\alpha) \qquad y_a \to \infty \ , \tag{4.28}$$

where $\alpha = (L/(2\pi\nu)+1)/2 - N(L)$. Obviously $\alpha \leq 1$ and it is precisely 1 only when L is $L = (2n+1)2\pi\nu$. Next it can be shown that for y_a much larger than $y_{N(L)}$ but not infinite the following is true:

$$\frac{dy_a}{dt} > \lim_{y_a\to\infty}\frac{dy_a}{dt} \quad x_a = 0 \tag{4.29}$$

$$\frac{dy_a}{dt} < \lim_{y_a\to\infty}\frac{dy_a}{dt} \quad x_a = \pi \tag{4.30}$$

We learn from these results that there exist values of L for which a pole that is added at infinity will have marginal attraction ($dy_a/dt = 0$). Similar understanding can be obtained from a standard stability analysis without using pole decomposition. Perturbing a TFH-cusp solution we find linear equations whose eigenvalues λ_i can be obtained by standard numerical techniques: (i) all $Re(\lambda_i)$ are non-positive. (ii) at the isolated values of L for which $L = (2n+1)2\pi\nu$ $Re(\lambda_1)$ and $Re(\lambda_2)$ become zero (note that due to the logarithmic scale the zero is not evident) (iii) There exists a general tendency of all $Re(\lambda_i)$ to approach zero in absolute magnitude such as $\frac{1}{L^2}$ from below as L increases. This indicates a growing sensitivity to noise when the system size increases. (iv) There exists a Goldsone mode $\lambda_0 = 0$ due to translational invariance.

The upshot of this discussion is that finite perturbations (i.e. poles at finite y_a) will grow if the x position of the pole is sufficiently near the tip. The position $x = \pi$ (the tip of the finger) is the most unstable one. In the channel geometry this means that noise results in the appearance of new cusps at the tip of the fingers, but due to the attraction to the giant cusp they move toward $x = 0$ and disappear in the giant cusp. In fact, one sees in numerical simulations a train of small cusps that move toward the giant cusp. Analysis shows that at the same time the furthest pole at $y_{N(L)}$ is pushed towards infinity. Also in cylindrical geometry the most sensitive position to the appearance of new cusps is right between two existing cusps independently if the system is marginal (the total number of poles fits the radius) or unstable (total number of poles is too small at a given radius). Whether or not the addition of a new pole results in tip splitting depends on their x position. When the distance from existing cusps is larger than $\mathcal{L}$ the new poles that are generated by noise will remain near the tip between the two cusps and will cause tip splitting.

The picture used remains valid as long as the poles that are introduced by the noisy perturbation do not destroy the identity of the giant cusp. Indeed, the numerical simulations show that in the presence of moderate noise the additional poles appear as smaller cusps that are constantly running towards the giant cusp. Our point here, is not to predict the numerical

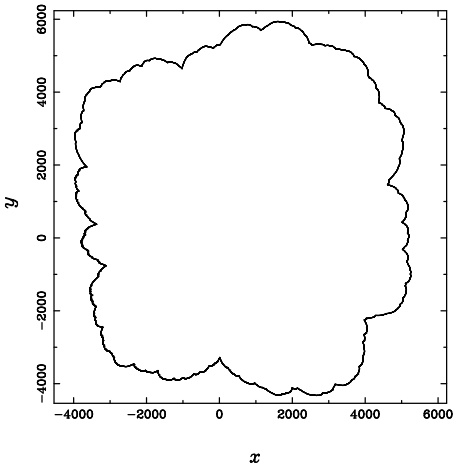

Figure 4.1: Simulations of the outward propagating flame front. Note that there is a wide distribution of cusp sizes.

values of the scaling exponents in the *channel* (this was done in ref. [17] and chapter 2, but to use them to predict the scaling exponents characterizing the acceleration and the geometry of the flame front in *radial* geometry.

Superficially it seems that in radial geometry the growth pattern is qualitatively different. In fact, close observation of the growth patterns (see Fig.4.1) shows that most of the time there exist some big cusps that attract other smaller cusps, but that every now and then "new" big cusps form and begin to act as local absorbers of small cusps that appear randomly. The understanding of this phenomenon gives the clue how to translate results from channels to radial growth.

Equations (4.9), (4.10) again admit exact solutions in terms of poles, of the form of Eq.(4.13). It is easy write down the equations of motion of the poles and check that the poles are attractive along the real direction (which means physically that they are attracted along the angular coordinate) but they are repulsive along the imaginary direction, which is associated with the radial coordinate. If it were not for the stretching that is caused by the increase of the radius (and with it the perimeter), all the poles would have coalesced into one giant cusp. Thus we have a competition between pole attraction and stretching. Since the attraction decreases with the distance between the poles in the angular directions, there is always an initial critical length scale above which poles cannot coalesce their real coordinates when time progresses.

Suppose now that noise adds new poles to the system. The poles do not necessarily merge their real positions with existing cusps. If we have a large cusp made from the merging of the real coordinates x_c of N_c poles, we want to know whether a nearby pole with real coordinate x_1 will merge with this large cusp. The answer will depend of course on the distance $D \equiv r_0|x_c - x_1|$. A direct calculation [19], using the equation of motions for the

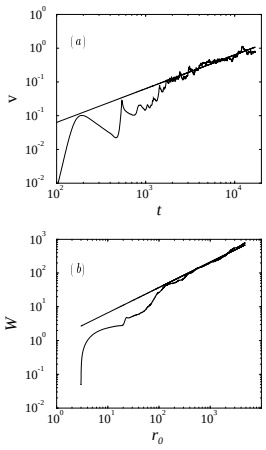

Figure 4.2: Panel a: a logarithmic plot of the velocity versus time for a radially evolving system. The parameters of the simulation are: $f = 10^{-8}, \gamma = 0.8, \nu = 1$. Panel b:Logarithmic plot of the width of the flame front as a function of the mean radius.

poles shows that there exists a critical length $\mathcal{L}(r_0)$ such that if $D > \mathcal{L}(r_0)$ the single pole never merges with the giant cusp. The result of the calculation is that

$$\mathcal{L} \sim r_0^{1/\beta} \ . \tag{4.31}$$

Note that a failure of a single pole to be attracted to a large cusp means that tip-splitting has occurred. This is the exact analog of tip-splitting in Laplacian growth.

It is now time to relate the channel and radial geometries. We identify the typical scale in the radial geometry as $\mathcal{L} \sim W \sim r_0^{\chi}$. On the one hand this leads to the scaling relation $\beta = 1/\chi$. On the other hand we use the result established in a channel, (4.26), with this identification of a scale, and find $\dot{r}_0 = r_0^{\chi\mu}$. Comparing with (4.7) we find:

$$\beta = \frac{1}{(1 - \chi\mu)} \ . \tag{4.32}$$

This result leads us to expect two dynamical regimes for our problem. Starting from smooth initial conditions, in relatively short times the roughness exponent remains close to unity. This is mainly since the typical scale $\mathcal{L}$ is not relevant yet, and most of the poles that are generated by noise merge into a few larger cusps. In later times the roughening exponent settles at its asymptotic value, and all the asymptotic scaling relations used above become valid. We thus expect β to decrease from $1/(1-\mu)$ to an asymptotic value determined by $\chi = 1/\beta$ in (4.32):

$$\beta = 1 + \mu \approx 1.35 \pm 0.03 \ . \tag{4.33}$$

The expected value of χ is thus $\chi = 0.74 \pm 0.03$. We tested these predictions in numerical

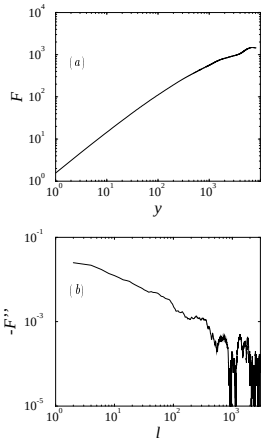

Figure 4.3: Panel a: a logarithmic plot of the correlation function F(y) of the interface versus the distance y between points. Panel b: Second derivative of the correlation function -F"(l) of the interface versus the distance l between points.

simulations. We integrated Eq.(4.24), and in Fig.4.2 we display the results for the growth velocity as a function of time. After a limited domain of exponential growth we observe a continuous reduction of the time dependent exponent. In the initial region we get $\beta = 1.65 \pm 0.1$ while in the final decade of the temporal range we find $\beta = 1.35 \pm 0.1$. We consider this a good agreement with (4.33). A second important test is provided by measuring the width of the system as a function of the radius, see Fig.4.2b. Again we observe a cross-over related to the initial dynamics; In the last temporal decade the exponent settles at $\chi = 0.75 \pm .1$. We conclude that at times large enough to observe the asymptotics our predictions are verified.

Finally, we stress some differences between radial and channel geometries. Fronts in a channel exhibit mainly one giant cusp which is only marginally disturbed by the small cusps that are introduced by noise. In the radial geometry, as can be concluded from the discussion above, there exist at any time cusps of all sizes from the smallest to the largest. This broad distribution of cusps (and scales) must influence correlation function in ways that differ qualitatively from correlation functions computed in channel geometries. To make the point clear we exhibit in Fig.4.3a the structure function

$$F(y) \equiv \sqrt{\langle |R(x+y) - R(x)|^2 \rangle} \tag{4.34}$$

computed for a typical radial front, with $x = R\theta$. To stress the scaling region we exhibit the second derivative of this function in Fig.4.3b. The low end of the graph can be fitted well by a power law $y^{-\alpha}$ with $\alpha \approx 0.6$. This indicates that $F(y) \approx Ay + By^{2-\alpha}$. In a channel geometry we get entirely different structure functions that do not exhibit such scaling functions at all. The way to understand this behavior in the radial geometry is to consider a distribution

of cusps that remain distinct from each other but whose scales are distributed according to some distribution $P'(\ell)$. Let us define a distribution function $P(\ell) \sim \ell P'(\ell)$ which give us the probability that a point on the circuit with the mean radius lies on the basis of the cusp with the size ℓ. For each of these cusps there is a contribution to the correlation function of the form $f(y,\ell) \approx \ell g(y/\ell)$ where $g(x)$ is a scaling function, $g(x) \approx x$ for $x < 1$ and $g(x) \approx$ constant for $x > 1$. The total correlation can be estimated (when the poles are distinct) as

$$F(y) \approx \sum_{\ell} P(\ell)\ell g(y/\ell) \ . \tag{4.35}$$

The first derivative leaves us with $\sum_\ell P(\ell)g'(y/\ell)$, and using the fact that g' vanishes for $x > 1$ we estimate $F'(y) = \sum_{\ell=y}^{W} P(\ell)$. The second derivative yields $F''(y) \approx -P(y)$. Thus the structure function is determined by the scale distribution of cusps, and if the latter is a power law, this should be seen in the second derivative of $F(y)$ as demonstrated in Fig.4.3. The conclusion of this analysis is that the radial case exhibits a scaling function that characterizes the distributions of cusps, $P(\ell) \approx \ell^{-\alpha}$.

4.3 Conclusions

The main purpose of this chapter was to find exponents of the problem and find connections between them. Using the main result of the channel case (dependence of the velocity on the ch annel size) we can find the acceleration of the flame front in the radial case ($R_0(t) = (const + t)^\beta$)

$$\beta = 1 + \mu \ . \tag{4.36}$$

where μ is the exponent for the dependence of the velocity on the channel size found before, β is the acceleration exponent and R_0 is a mean radius of the flame front.

Dependence of the width of the flame front in the radial case $W(t)$ on mean radius ($R_0(t) = (const + t)^\beta$) is

$$W(t) \sim R_0(t)^\chi \ . \tag{4.37}$$

$$\chi = 1/\beta \ . \tag{4.38}$$

In summary, we demonstrated that it is possible to use information about noisy channel dynamics to predict nontrivial features of the radial evolution, such as the acceleration and roughening exponents. It would be worthwhile to examine similar ideas in the context of Laplacian growth patterns.

Chapter 5

Laplacian Growth

5.1 Introduction

The problem of pattern formation is one of the most rapidly developing branches of nonlinear science today [1]. Of special interest is the study of the front dynamics between two phases (interface) that arises in a variety of nonequilibrium physical systems. If, as it usually happens, the motion of the interface is slow in comparison with the processes that take place in the bulk of both phases (such as heat transfer, diffusion, etc.), the scalar field governing the evolution of the interface is a harmonic function. It is natural then, to call the whole process *Laplacian growth*. Depending on the system, this harmonic scalar field is a temperature (in the freezing of a liquid or Stefan problem), a concentration (in solidification from a supersaturated solution), an electrostatic potential (in electrodeposition), a pressure (in flows through porous media), a probability (in diffusion-limited aggregation), etc.

The mathematical problem of Laplacian growth without surface tension exhibits a family of exact (analytic) solutions in terms of logarithmic poles in the complex plane. We show that this family of solutions has a remarkable property: generic initial conditions in channel geometry which begin with arbitrarily many features exhibit an inverse cascade into a single finger.

In the absence of surface tension, whose effect is to stabilize the short-wavelength perturbations of the interface, the problem of 2D Laplacian growth is described as follows

$$(\partial_x^2 + \partial_y^2)u = 0 \ . \tag{5.1}$$

$$u \mid_{\Gamma(t)} = 0 \ , \partial_n u \mid_{\Sigma} = 1 \ . \tag{5.2}$$

$$v_n = \partial_n u \mid_{\Gamma(t)} \ . \tag{5.3}$$

Here $u(x, y; t)$ is the scalar field mentioned, $\Gamma(t)$ is the moving interface, Σ is a fixed external boundary, ∂_n is a component of the gradient normal to the boundary (i.e. the normal derivative), and v_n is a normal component of the velocity of the front.

We consider an infinitely long interface, obtained by a periodic continuation of the interface in the channel with periodic boundary conditions.Then We introduce a time-dependent conformal map f from the lower half of a "mathematical" plane, $\xi \equiv \zeta + i\eta$, to the domain

of the physical plane, $z \equiv x + iy$, where the Laplace equation 5.1 is defined as $\xi \xrightarrow{f} z$. We also require that $f(t,\xi) \approx \xi$ for $\xi \longrightarrow \zeta - i\infty$. Thus the function $z = f(t,\zeta)$ describes the moving interface. From Eqs. (5.1), (5.2), (5.3) for function $f(t,\xi)$ we obtain the *Laplacian Growth Equation*

$$Im(\frac{\partial f(\xi,t)}{\partial \xi}\overline{\frac{\partial f(\xi,t)}{\partial t}}) = 1 \mid_{\xi=\zeta-i0} , f_\zeta \mid_{\zeta-i\infty} = 1 \ . \tag{5.4}$$

Now we will extend these results obtained for periodic boundary conditions to the more physical "no-flux" boundary conditions (no flux across the lateral boundaries of the channel). This requires that the moving interface orthogonally intersects the walls of the channel. However, unlike the case of periodic boundary conditions, the end points at the two boundaries do not necessarily have the same horizontal coordinate. This is also a periodic problem where the period equals twice the width of the channel. The analysis is the same as before, but now only half of the strip should be considered as the physical channel, whereas the second half is the unphysical mirror image.

Let us look for a solution of Eq. (5.4) in the next form

$$\begin{aligned} &f(\xi,t) = \lambda\xi - i\tau(t) - i\sum_{l=1}^{N}\alpha_l \log(e^{i\xi} - e^{i\xi_l(t)}), \\ &\sum_{l=1}^{N}\alpha_l = 1-\lambda, -1 < \lambda < 1 \ , \end{aligned} \tag{5.5}$$

where $\tau(t)$ is some real function of time, λ is a real constant, α_l is a complex constant, $\xi_l = \zeta_l + i\eta_l$ denotes the position of the pole with the number l and N is the number of poles.

For the "no-flux" boundary condition we must add the condition that for every pole $\xi_l = \zeta_l + i\eta_l$ with α_l exists a pole $\xi_l = -\zeta_l + i\eta_l$ with $\overline{\alpha_l}$. So for the function $F(i\xi,t) = if(\xi,t)$

$$\overline{F(i\xi,t)} = F(\overline{i\xi},t) \tag{5.6}$$

We want to prove that the final state will be only one finger.

5.2 Asymptotic behavior of the poles in the mathematical plane

The main purpose of this chapter is to investigate the asymptotic behavior of the poles in the mathematical plane. We want to demonstrate that for time $t \mapsto \infty$, all poles go to a single point (or two points for no-flux boundary conditions). The equation for the interface is

$$\begin{aligned} &f(\xi,t) = \lambda\xi - i\tau(t) - i\sum_{l=1}^{N}\alpha_l \log(e^{i\xi} - e^{i\xi_l(t)}), \\ &\sum_{l=1}^{N}\alpha_l = 1-\lambda, -1 < \lambda < 1 \ . \end{aligned} \tag{5.7}$$

By substitution of Eq. (5.7) in the *Laplacian Growth Equation*

$$Im(\frac{\partial f(\xi,t)}{\partial \xi}\overline{\frac{\partial f(\xi,t)}{\partial t}}) = 1 \mid_{\xi=\zeta-i0} , \tag{5.8}$$

we can find the equations of pole motion:

$$const = \tau(t) + (1 - \sum_{k=1}^{N} \overline{\alpha_k}) \log \frac{1}{a_l} + \sum_{k=1}^{N} \overline{\alpha_k} \log(\frac{1}{a_l} - \overline{a_k}) \tag{5.9}$$

and

$$\tau = t - \frac{1}{2} \sum_{k=1}^{N} \sum_{l=1}^{N} \overline{\alpha_k} \alpha_l \log(1 - \overline{a_k} a_l) + C_0 , \tag{5.10}$$

where $a_l = e^{i\xi_l}$.

From eq. (5.9) we can find

$$C_1 = (1-\lambda)\tau - \sum_{l=1}^{N} \alpha_l \log a_l + \sum_{k=1}^{N} \sum_{l=1}^{N} \overline{\alpha_k} \alpha_l \log(1 - \overline{a_k} a_l) . \tag{5.11}$$

From eqs. (5.10) and (5.11) we can obtain

$$Im(\sum_{l=1}^{N} \alpha_l \log a_l) = constant \tag{5.12}$$

and

$$t = (\frac{1+\lambda}{2})\tau + \frac{1}{2} Re(\sum_{l=1}^{N} \alpha_l \log a_l) + C_1/2 , \tag{5.13}$$

where α_l is a constant, $\xi_l(t)$ is the position of the poles, $a_l = e^{i\xi_l(t)}$, and $\frac{\lambda+1}{2}$ is the portion of the channel occupied by the moving liquid. We will see that for $\tau \mapsto \infty$ we obtain one finger with wide $\frac{\lambda+1}{2}$.

In Appendix A we will prove from eq.(5.10) that $\tau \mapsto \infty$, if $t \mapsto \infty$ and if any finite time singularity does not exist.

The equations of pole motion are next from eq. (5.9)

$$const = \tau + i\overline{\xi_k} + \sum_{l} \alpha_l \log(1 - e^{i(\xi_l - \overline{\xi_k})}), \tag{5.14}$$

$$const = \zeta_k + \sum_{l} (\alpha_l'' \log \mid 1 - e^{i(\xi_l - \overline{\xi_k})} \mid + \alpha_l' \arg(1 - e^{i(\xi_l - \overline{\xi_k})})), \tag{5.15}$$

$$const = \tau + \eta_k + \sum_{l} (\alpha_l' \log \mid 1 - e^{i(\xi_l - \overline{\xi_k})} \mid - \alpha_l'' \arg(1 - e^{i(\xi_l - \overline{\xi_k})})), \tag{5.16}$$

$$\xi_l = \zeta_l + i\eta_l, \eta_l > 0 . \tag{5.17}$$

$$\alpha_l = \alpha_l' + i\alpha_l'' \tag{5.18}$$

Let us examine

$$\arg(1-e^{i(\xi_l-\overline{\xi_k})})=\arg([1-e^{i(\zeta_l-\zeta_k)}e^{-(\eta_l+\eta_k)}])=\arg[1-a_{lk}e^{i\varphi_{lk}}] \tag{5.19}$$

$$\varphi_{lk}=\zeta_l-\zeta_k, a_{lk}=e^{-(\eta_l+\eta_k)} \tag{5.20}$$

$\arg[1-a_{lk}e^{i\varphi_{lk}}]$ is a singlevalued function of φ_{lk}, i.e.

$$-\frac{\pi}{2}\le\arg[1-a_{lk}e^{i\varphi_{lk}}]\le\frac{\pi}{2}\ . \tag{5.21}$$

From the eq. (5.16) the only way to compensate for the divergence of term τ is that $\eta_k\mapsto 0$ for $\tau\mapsto\infty, 1\le k\le N$.

We want to investigate asymptotic behavior of poles $\tau\mapsto\infty$. To eliminate the divergent term $\log\mid 1-e^{i(\xi_k-\overline{\xi_k})}\mid$ we multiply eq. (5.16) by α_k'' and eq. (5.15) by α_k' and take difference

$$\begin{aligned}const=\alpha_k'\zeta_k-\alpha_k''\tau+\sum_{l\neq k}((\alpha_l''\alpha_k'-\alpha_k''\alpha_l')\log\mid 1-e^{i(\xi_l-\overline{\xi_k})}\mid+\\ (\alpha_l'\alpha_k'+\alpha_l''\alpha_k'')\arg(1-e^{i(\xi_l-\overline{\xi_k})})).\end{aligned} \tag{5.22}$$

We have the divergent terms $\alpha_k''\tau$ in this equation. We may assume that for $t\mapsto\infty$, N' groups of poles exist to eliminate the divergent terms ($\varphi_{lk}\mapsto 0$ for all members of a group). N_l is the number of poles in each group, $1<l<N'$. For each group by summation of eqs. (5.22) over all group poles we obtain

$$\begin{aligned}const=\alpha_k^{gr\prime}\zeta_k^{gr}-\alpha_k^{gr\prime\prime}\tau+\sum_{l\neq k}((\alpha_l^{gr\prime\prime}\alpha_k^{gr\prime}-\alpha_k^{gr\prime\prime}\alpha_l^{gr\prime})\log\mid 1-e^{i(\xi_l^{gr}-\overline{\xi_k^{gr}})}\mid+\\ (\alpha_l^{gr\prime}\alpha_k^{gr\prime}+\alpha_l^{gr\prime\prime}\alpha_k^{gr\prime\prime})\arg(1-e^{i(\xi_l^{gr}-\overline{\xi_k^{gr}})})).\end{aligned} \tag{5.23}$$

$$\alpha_l^{gr\prime\prime}=\sum_k^{N_l}\alpha_k''\ , \tag{5.24}$$

$$\alpha_l^{gr\prime}=\sum_k^{N_l}\alpha_k'\ . \tag{5.25}$$

We have no merging of these groups for large τ and we investigate the motion of poles with this assumption

$$\mid\zeta_l^{gr}-\zeta_k^{gr}\mid\gg\eta_l^{gr}+\eta_k^{gr}, 1\le l,k\le N\ . \tag{5.26}$$

For $l\neq k$, $\eta_k^{gr}\mapsto 0$, $\varphi_{lk}^{gr}=\zeta_l^{gr}-\zeta_k^{gr}$ we obtain

$$\log\mid 1-e^{i(\xi_l^{gr}-\overline{\xi_k^{gr}})}\mid\approx\log\mid 1-e^{i(\zeta_l^{gr}-\zeta_k^{gr})}\mid=\log 2+\frac{1}{2}\log\sin^2\frac{\varphi_{lk}^{gr}}{2} \tag{5.27}$$

and

$$\arg(1-e^{i(\xi_l^{gr}-\overline{\xi_k^{gr}})})\approx\arg(1-e^{i(\zeta_l^{gr}-\zeta_k^{gr})})=\frac{\varphi_{lk}^{gr}}{2}+\pi n-\frac{\pi}{2}\ . \tag{5.28}$$

We choose n in Eq.(5.28) so that Eq.(5.21) is correct.
Substituting these results to the eqs. (5.23) we obtain

$$C_k = \alpha^{gr\prime}\zeta_k^{gr} - \alpha_k^{gr\prime\prime}\tau + \sum_{l\neq k}[(\alpha_l^{gr\prime\prime}\alpha_k^{gr\prime} - \alpha_k^{gr\prime\prime}\alpha_l^{gr\prime})\log \mid \sin\frac{\varphi_{lk}^{gr}}{2} \mid$$
$$+(\alpha_l^{gr\prime}\alpha_k^{gr\prime} + \alpha_l^{gr\prime\prime}\alpha_k^{gr\prime\prime})\frac{\varphi_{lk}^{gr}}{2}] \tag{5.29}$$

5.3 Theorem about coalescence of the poles

From eqs. (5.29) we can conclude
(i) By summation of eqs.(5.29) (or exactly from eq. (5.12)) we obtain

$$\sum_k \alpha_k^{gr\prime}\zeta_k^{gr} = const\ . \tag{5.30}$$

(ii) For $\mid \varphi_{lk}^{gr} \mid \mapsto 0, 2\pi$, we obtain $\log \mid \sin\frac{\varphi_{lk}^{gr}}{2} \mid \mapsto \infty$, meaning that the poles can not pass off each other;
(iii) From (ii) we conclude that $0 <\mid \varphi_{lk}^{gr} \mid < 2\pi$
(iv) From (i) and (iii), $\zeta_k^{gr} \mapsto \infty$ is impossible;
(v) In eq.(5.29) we must compensate the second divergent term. From (iv) and (iii) we can do it only if $\alpha_l^{gr\prime\prime} = \sum_k^{N_l} \alpha_k'' = 0$ for all l.
So from eq. (5.29) we obtain

$$\sum_k^{N_l} \alpha_k'' = 0\ , \tag{5.31}$$

$$\dot{\varphi_{lk}^{gr}} = 0\ , \tag{5.32}$$

$$\varphi_{lk}^{gr} \neq 0\ , \tag{5.33}$$

$$\dot{\zeta_k^{gr}} = 0\ . \tag{5.34}$$

For the asymptotic motion of poles in the group N_m we obtain from eqs. (5.31), (5.32), (5.33), (5.34) taking leadind terms in eqs. (5.13), (5.14)

$$\tau = \frac{2}{\lambda+1}t\ , \tag{5.35}$$

$$0 = \dot{\tau} + \sum_l^{N_m} \alpha_l \frac{\dot{\eta_k} + \dot{\eta_l} + i(\dot{\zeta_k} - \dot{\zeta_l})}{\eta_k + \eta_l + i(\zeta_k - \zeta_l)}\ . \tag{5.36}$$

The solution to these equations is

$$\eta_k = \eta_k^0 e^{-\frac{1}{\alpha_m^{gr\prime}}\frac{2}{1+\lambda}t}\ , \tag{5.37}$$

$$\varphi_{lk} = {\varphi_{lk}}^0 e^{-\frac{1}{\alpha_m^{gr\prime}}\frac{2}{1+\lambda}t} \ , \tag{5.38}$$

$$\dot{\zeta_k} = 0 \ . \tag{5.39}$$

So we may conclude that for eliminating the divergent term we need

$$\alpha_l^{gr\prime\prime} = \sum_k^{N_l} \alpha_k'' = 0, \tag{5.40}$$

$$\alpha_l^{gr\prime}(1+\lambda) > 0 \tag{5.41}$$

for all l.

5.4 Conclusions

With the periodic boundary condition, eq.(5.40) is correct for all poles, so we obtain $N' = 1$, $m = 1$ and $N_m = N$.

Therefore the unique solution is

$$\eta_k = \eta_k^0 e^{-\frac{2}{(1-\lambda^2)}t} \ , \tag{5.42}$$

$$\varphi_{lk} = {\varphi_{lk}}^0 e^{-\frac{2}{(1-\lambda^2)}t} \ , \tag{5.43}$$

$$\dot{\zeta_k} = 0 \ . \tag{5.44}$$

$$1 - \lambda^2 > 0 \tag{5.45}$$

With the no-flux boundary condition we have a pair of the poles whose condition of eq. (5.40) is correct so all these pairs must merge. Because of the symmetry of the problem these poles can merge only on the boundaries of the channel $\zeta = 0, \pm\pi$. Therefore we obtain two groups of the poles on boundaries $N' = 2$, $m = 1, 2$, $N_1 + N_2 = N$, $\alpha_1^{gr\prime} + \alpha_2^{gr\prime} = 1 - \lambda$.

Consequently we obtain the solution (on two boundaries):

$$\eta_k^{(1)} = \eta_k^{(1),0} e^{-\frac{1}{\alpha_1^{gr\prime}}\frac{2}{1+\lambda}t} \ , \tag{5.46}$$

$$\varphi_{lk}^{(1)} = {\varphi_{lk}}^{(1),0} e^{-\frac{1}{\alpha_1^{gr\prime}}\frac{2}{1+\lambda}t} \ , \tag{5.47}$$

$$\zeta_k^{(1)} = 0 \ ; \tag{5.48}$$

$$\eta_k^{(2)} = \eta_k^{(2),0} e^{-\frac{1}{\alpha_2^{gr\prime}}\frac{2}{1+\lambda}t} \ , \tag{5.49}$$

$$\varphi_{lk}^{(2)} = {\varphi_{lk}}^{(2),0} e^{-\frac{1}{\alpha_2^{gr\prime}}\frac{2}{1+\lambda}t} \ , \tag{5.50}$$

$$\zeta_k^{(2)} = \pm\pi \ ; \tag{5.51}$$

$$\alpha_1^{gr\prime}(1+\lambda) > 0, \tag{5.52}$$

$$\alpha_2^{gr\prime}(1+\lambda) > 0. \tag{5.53}$$

5.5 Appendix A

We need to prove that $\tau \mapsto \infty$, if $t \mapsto \infty$ and if any finite time singularity does not exist. This is apparent if the second term in the next formula for τ is greater than zero:

$$\tau = t + [-\frac{1}{2}\sum_{k=1}^{N}\sum_{l=1}^{N}\overline{\alpha_k}\alpha_l \log(1-\overline{a_k}a_l)] + C_0 \ , \tag{5.54}$$

where $\mid a_l \mid < 1$ for all l. Let us prove it.

$$\begin{aligned}
&-\frac{1}{2}\sum_{k=1}^{N}\sum_{l=1}^{N}\overline{\alpha_k}\alpha_l \log(1-\overline{a_k}a_l) = -\frac{1}{2}\sum_{k=1}^{N}\sum_{l=1}^{N}\overline{\alpha_k}\alpha_l \sum_{n=1}^{\infty}(-\frac{(\overline{a_k}a_l)^n}{n}) \\
&\frac{1}{2}\sum_{n=1}^{\infty}\frac{1}{n}(\sum_{k=1}^{N}\overline{\alpha_k}(\overline{a_k})^n)(\sum_{l=1}^{N}\alpha_l(a_l)^n) \\
&= \frac{1}{2}\sum_{n=1}^{\infty}\frac{1}{n}\overline{(\sum_{l=1}^{N}\alpha_l(a_l)^n)}(\sum_{l=1}^{N}\alpha_l(a_l)^n) > 0
\end{aligned} \tag{5.55}$$

Chapter 6

Summary

The problem of flame propagation is studied as an example of unstable fronts that wrinkle on many scales. The analytic tool of pole expansion in the complex plane is employed to address the interaction of the unstable growth process with random initial conditions and perturbations. We argue that the effect of random noise is immense and that it can never be neglected in sufficiently large systems. We present simulations that lead to scaling laws for the velocity and acceleration of the front as a function of the system size and the level of noise, and analytic arguments that explain these results in terms of the noisy pole dynamics.

We consider flame front propagation in channel geometries. The steady state solution in this problem is space dependent, and therefore the linear stability analysis is described by a partial integro-differential equation with a space dependent coefficient. Accordingly it involves complicated eigenfunctions. We show that the analysis can be performed to required detail using a finite order dynamical system in terms of the dynamics of singularities in the complex plane, yielding detailed understanding of the physics of the eigenfunctions and eigenvalues.

The roughening of expanding flame fronts by the accretion of cusp-like singularities is a fascinating example of the interplay between instability, noise and nonlinear dynamics that is reminiscent of self-fractalization in Laplacian growth patterns. The nonlinear integro-differential equation that describes the dynamics of expanding flame fronts is amenable to analytic investigations using pole decomposition. This powerful technique allows the development of a satisfactory understanding of the qualitative and some quantitative aspects of the complex geometry that develops in expanding flame fronts.

Flame Propagation is used as a prototypical example of expanding fronts that wrinkle without limit in radial geometries but reach a simple shape in channel geometry. We show that the relevant scaling laws that govern the radial growth can be inferred once the simpler channel geometry is understood in detail. In radial geometries (in contrast to channel geometries) the effect of external noise is crucial in accelerating and wrinkling the fronts. Nevertheless, once the interrelations between system size, velocity of propagation and noise level are understood in channel geometry, the scaling laws for radial growth follow.

The mathematical problem of Laplacian growth without surface tension exhibits a family of exact (analytic) solutions in terms of logarithmic poles in the complex plane. We show that this family of solutions has a remarkable property: generic initial conditions in channel geometry which begin with arbitrarily many features exhibit an inverse cascade into a single finger.

Bibliography

[1] P. Pelce, *Dynamics of Curved Fronts*, (Academic press, Boston (1988))

[2] A.-L. Barbási and H.E. Stanley, *Fractal Concepts in Surface Growth* (Cambridge University Press, 1995).

[3] T. Viscek *Fractal Growth Phenomena* (World Scientific, Singapore, 1992)

[4] T. A. Witten, Jr. and L.M. Sander, Phys. Rev. Lett. **47**, 1400 (1981)

[5] J.W. Evans, Rev. Mod. Phys. **65**, 1281 (1993)

[6] S. Ponce Dawson and M. Mineev-Weinstein, Physica D **73**, 373 (1994)

[7] M. Mineev-Weinstein and S. Ponce Dawson, Phys. Rev. E **50**, R24 (1994)

[8] M. Mineev-Weinstein, Phys. Rev. Lett. **80**, 2113 (1998)

[9] G. Sivashinsky, Acta Astronautica **4**, 1177 (1977).

[10] Yu.A. Gostintsev, A.G. Istratov and Yu.V. Shulenin, Combust. Expl. Shock Waves **24**, 70 (1989)

[11] L. Filyand, G.I. Sivahshinsky and M.L. Frankel, Physica **D 72**, 110 (1994)

[12] O. Thual, U.Frisch and M. Henon, J. Physique, **46**, 1485 (1985).

[13] S. Gutman and G. I. Sivashinsky, Physica D**43**, 129 (1990).

[14] D. Bessis and J.D. Fournier J. Physique Lett., **45**, L-833 (1984).

[15] G. Joulin, J. Phys. France, **50**, 1069 (1989).

[16] G. Joulin, Phys.Rev **E50**, 2030 (1994)

[17] Z. Olami, B. Glanti, O. Kupervasser and I. Procacccia , Random Noise and Pole-Dynamics in Unstable Front Propagation, Phys. Rev. E. **55** (3), 2649 (1997).

[18] O. Kupervasser, Z. Olami and I. Procaccia Stability Analysis of Flame Fronts: Dynamical Systems Approach in the Complex Plane, accepted for publication to Phys. Rev. E

[19] O. Kupervasser, Z. Olami and I. Procacccia, Geometry of Developing Flame Fronts:Analysis with Pole Decomposition, ,Phys. Rev. Lett. **76**, 146 (1996).

[20] B. Glanti, O. Kupervasser, Z. Olami and I. Procacccia, Dynamics and Wrinkling of Radially Propagation Fronts Inferred from Scaling Law in Channel Geometries, Phys. Rev. Lett., **80**, 11 (1998)

[21] M. Mineev-Weinstein, O. Kupervasser, Formation of a Single Saffman-Taylor Finger after Fingers Competition An Exact Result in the Absence of Surface Tension, in preparation.

[22] M. Rahibe, N. Aubry, G.I. Sivashinsky and R. Lima, Formation of wrinkles in outwardly propagating flames, Phys. Rev. E **52** (4), 3675 (1995)

[23] M. Rahibe, N. Aubry and G.I. Sivashinsky, Stability of pole solution for planar propogating flames, Phys. Rev. E **54** (3), 4958 (1996)

[24] M. Rahibe, N. Aubry and G.I. Sivashinsky, Instability of pole solutions for planar propagating flames in sufficiently large domains, Combust. Theory Modelling **2**, 19 (1998)

[25] Wm T Ashurst, Darrieus-Landau instability, growing cycloids and expanding flame acceleration, Combust. Theory Modelling **1**, 405 (1997)

[26] Y. Kortsarts, I.Brailovsky and G.I. Sivashinsky, On Hydrodynamic Instability of Stretched Flames, Combust. Sci. Tech. **123**, 207 (1997)

[27] Guy Joulin and Pierre Cambray, On a Tentative, Approximate Evolution Equation for Markedly Wrinkled Premixed Flames, Combust. Sci. Tech. **81**, 243 (1992)

[28] Pierre Cambray and Guy Joulin, Length-Scales of Wrinkling of Weakly-Forced, Unstable Premixed Flames, Combust. Sci. Tech. **97**, 405 (1994)

[29] P. Cambray, K. Joulain and G. Joulin, Mean Evolution of Wrinkle Wavelengths in a Model of Weakly-Turbulent Premixed Flame, Combust. Sci. Tech. **103**, 265 (1994)

[30] Guy Joulin, Nonlinear Hydrodynamic instability of expanding flames: Intrinsic dynamics, Phys. Rev. E, **50** (3), 2030 (1994)

[31] T.A. Witten and L.M. Sander, Phys.Rev. Lett. **47**, 1400 (1981).

[32] P.Meakin, Phys.Rep. **235**, 189 (1993).

[33] T. Halpin-Healey and Y.C. Zhang, Phys. Rep. **254**, 215 (1995).

[34] Y. Kuramoto, Suppl.Prog.Theor.Phys **64**,346 (1978).

[35] B.Shraiman and D. Bensimon, Phys.Rev. **A30**,2840 (1984)

[36] S. D. Howison, J. Fluid Mech. **167**, 439 (1986)

[37] L. Landau, Acta Physiochimica U.R.S.S. **19**, 77 (1944)

[38] Y. C. Lee and H. H Chen, Phys. Scr.,**T 2**,41 (1982).

[39] G. Joulin, Zh.Eksp. Teor. Fiz., **100**, 428 (1990).

[40] B. Galanti, P.L. Sulem and A.D. Gilbert, Physica D **47**, 416(1991). and in the references therein.

[41] H. Risken, *The Fokker -Planck Equation* (Springer, Berlin 1984), p.124 Eq.(5.110)

[42] V.S. L'vov and I. Procaccia, Phys.Rev.Let. **69**, 3543, (1992).

[43] L. Landau, Acta Physiochimica U.R.S.S. **19**, 77 (1944)

[44] D.A. Kessler, J. Koplik and H. Levine ,Adv. Phys. **37**, 255-339 (1986)